

Global-local shrinkage priors for modeling random effects in multivariate spatial small area estimation

Shushi Nishina¹, Takahiro Onizuka² and Shintaro Hashimoto¹

¹ Department of Mathematics, Hiroshima University

² Graduate School of Social Sciences, Chiba University

January 22, 2026

Abstract

Small area estimation (SAE) plays a central role in survey statistics and epidemiology, providing reliable estimates for domains with limited sample sizes. The multivariate Fay-Herriot model has been extensively used for this purpose, because it enhances estimation accuracy by borrowing strength across multiple correlated variables. In this paper, we develop a Bayesian extension of the multivariate Fay-Herriot model that enables flexible, component-specific shrinkage of the random effects. The proposed approach employs global-local priors formulated through a sandwich mixture representation, allowing adaptive regularization of each element of the random-effect vectors. This construction yields greater robustness and prevents excessive shrinkage in areas exhibiting strong underlying signals. In addition, we incorporate spatial dependence into the model to account for geographical correlation across small areas. The resulting spatial multivariate framework simultaneously exploits cross-variable relationships and spatial structure, yielding improved estimation efficiency. The utility of the proposed method is demonstrated through simulation studies and an empirical application to real survey data.

Keywords: Horseshoe prior; Markov chain Monte Carlo; Multivariate Fay-Herriot model; Small area estimation; Spatial random effects

1 Introduction

Small area estimation (SAE) has become an indispensable framework in disciplines such as survey statistics and epidemiology, where reliable estimates are required for domains with limited or no reliable direct data (Rao and Molina, 2015; Sugawara and Kubokawa, 2020). Among various SAE approaches, the Fay-Herriot model (Fay and Herriot, 1979), a widely used area-level model, has been particularly influential due to its flexibility and computational efficiency. Multivariate extensions of the Fay-Herriot model have attracted growing attention, as they exploit correlations among multiple related variables to enhance estimation accuracy (Fay, 1987; Datta et al., 1998). Moreover, when spatial information is available, explicitly modeling spatial dependence can further improve estimation by incorporating geographic structure. Several spatially correlated versions of the Fay-Herriot model have been proposed (see, e.g., Porter et al., 2014, 2015; Chung and Datta, 2022; Tang and Ghosh, 2023; Wang et al., 2025); however, the integration of spatial dependence with flexible shrinkage mechanisms remains relatively under-explored.

An important aspect of SAE modeling lies in the specification and assessment of random effects. In many practical applications, certain areas may not require random effects; thus, over-shrinkage or inappropriate inclusion of such effects can lead to biased or inefficient estimators. Consequently, determining the presence or absence of random effects, or, more generally, allowing for flexible shrinkage, is crucial for enhancing model robustness and interpretability. There has been extensive research on testing for random effects within the univariate small area estimation framework. For example, Datta et al. (2011) proposed a test-based approach under the null hypothesis that the common random effect variance equals zero. Over the past decade, studies addressing the sparsity of random effect parameters in small area estimation have also emerged. Although the Fay-Herriot model assumes a common area-level variance component across all small areas, random effects may be unnecessary in many of them. This assumption can be particularly problematic when the number of small areas is very large. To address this issue, Datta and Mandal (2015) introduced a two-component mixture distribution for the random effect parameters, also known as the spike-and-slab prior (see also Chakraborty et al., 2016). Tang et al. (2018) further proposed the use of global-local shrinkage priors for univariate small

area estimation and established several theoretical properties of the resulting shrinkage factors. This approach builds upon the expanding literature on Bayesian shrinkage priors such as the horseshoe prior (Carvalho et al., 2010), normal-gamma prior (Griffin and Brown, 2010) and Dirichlet-Laplace prior (Bhattacharya et al., 2015) which provide a principled framework for borrowing strength while encouraging sparsity. More recently, Ghosh et al. (2022) extended the work of Tang et al. (2018) to a multivariate setting by introducing local parameters for each area, while Tang and Ghosh (2023) considered the application of global-local priors to spatial small area estimation with univariate response variables.

In this paper, we develop a new Bayesian framework for multivariate spatial small area estimation by introducing global-local shrinkage priors within the multivariate spatial Fay-Herriot model. The proposed approach enables adaptive and spatially informed regularization of random effects, providing a flexible mechanism for borrowing strength both across areas and across multiple correlated variables. Specifically, we construct a novel shrinkage prior that combines a sandwich scale-mixture representation with a multivariate conditional autoregressive (MCAR) structure. This hierarchical formulation introduces local parameters whose number equals the product of the dimension of the multivariate direct estimates, thereby achieving element-wise, spatially correlated shrinkage of the random-effect vectors. For modeling these local parameters, we mainly consider both the normal-gamma and horseshoe priors, representing two complementary regimes of sparsity: the horseshoe prior performs well under strong sparsity, whereas the normal-gamma prior may be more effective in moderately sparse settings. Importantly, the proposed framework is general and can accommodate alternative shrinkage priors according to the needs of the analysis. Our method extends and generalizes the work of Ghosh et al. (2022) by incorporating spatial dependence and adaptive shrinkage within a unified Bayesian structure. To the best of our knowledge, this is the first attempt to model random effects in multivariate spatial small area estimation using global-local shrinkage priors. This development fills an important methodological gap, as spatial small area models have traditionally relied on homogeneous random-effect structures that may be overly restrictive in high-dimensional or heterogeneous settings. We further develop a Markov chain Monte Carlo (MCMC) algorithm for posterior inference and demonstrate, through simulation studies, that the proposed method achieves improved estimation accuracy and robustness compared with ex-

isting approaches. Finally, we illustrate its practical utility using data from the West Census Region based on the 2022 five-year American Community Survey (ACS) on median household income and poverty rate.

The remainder of this paper is organized as follows. Section 2 provides a brief overview of the multivariate Fay-Herriot model and introduces the modeling of random effects using global-local shrinkage priors. In Section 3, we propose a new multivariate spatial Fay-Herriot model that incorporates shrinkage priors through a sandwich scale-mixture structure. Section 4 presents the results of numerical experiments, and Section 5 illustrates the proposed methodology through an application to real data. Finally, Section 6 concludes the paper with a discussion and possible directions for future research. R code implementing the proposed methods is available in the GitHub repository <https://github.com/Takahiro-Onizuka/GL-MCAR>.

2 Multivariate FH model and sparsity for random effects

We consider multivariate small area estimation based on area-level models. The multivariate Fay-Herriot (FH) model (Fay, 1987) is a multivariate extension of the Fay-Herriot model (Fay and Herriot, 1979). The multivariate FH model is defined by

$$\begin{aligned} \mathbf{y}_i &= \boldsymbol{\theta}_i + \boldsymbol{\varepsilon}_i, \quad \boldsymbol{\theta}_i = \mathbf{X}_i \boldsymbol{\beta} + \mathbf{u}_i, \quad \boldsymbol{\varepsilon}_i \sim \mathcal{N}_k(\mathbf{0}, \mathbf{V}_i), \\ \mathbf{u}_i &\sim \mathcal{N}_k(\mathbf{0}, \boldsymbol{\Psi}), \quad i = 1, \dots, m, \end{aligned} \tag{2.1}$$

where \mathbf{y}_i is a $k \times 1$ vector, \mathbf{X}_i is a $k \times s$ matrix, and $\boldsymbol{\beta}$ is a $s \times 1$ vector. \mathbf{V}_i is a known covariance matrix and $\boldsymbol{\Psi}$ is a $k \times k$ covariance matrix of the random effect vector \mathbf{u}_i . Let $\mathbf{y} = (\mathbf{y}_1^\top, \dots, \mathbf{y}_m^\top)^\top \in \mathbb{R}^{mk}$, $\mathbf{X} = (\mathbf{X}_1^\top, \dots, \mathbf{X}_m^\top)^\top \in \mathbb{R}^{mk \times s}$, $\mathbf{u} = (\mathbf{u}_1^\top, \dots, \mathbf{u}_m^\top)^\top \in \mathbb{R}^{mk}$ and $\boldsymbol{\varepsilon} = (\boldsymbol{\varepsilon}_1^\top, \dots, \boldsymbol{\varepsilon}_m^\top)^\top \in \mathbb{R}^{mk}$. The model is expressed as

$$\mathbf{y} = \mathbf{X}\boldsymbol{\beta} + \mathbf{u} + \boldsymbol{\varepsilon}, \quad \mathbf{u} \sim \mathcal{N}_{mk}(\mathbf{0}, \mathbf{I}_m \otimes \boldsymbol{\Psi}), \quad \boldsymbol{\varepsilon} \sim \mathcal{N}_{mk}(\mathbf{0}, \mathbf{V}),$$

where \otimes is Kronecker product of matrices and $\mathbf{V} = \text{block diag}(\mathbf{V}_1, \dots, \mathbf{V}_m) \in \mathbb{R}^{mk \times mk}$. We assume that \mathbf{X} is of full rank. For example, we consider the crop data analyzed by Battese et al. (1988), who studied the data using the nested error regression model. For the i th county, let y_{i1}

and y_{i2} be survey data of average areas of corn and soybean, respectively. Also let x_{i1} and x_{i2} be satellite data of average areas of corn and soybean, respectively. In this case, \mathbf{y}_i , \mathbf{X}_i and $\boldsymbol{\beta}$ correspond to

$$\mathbf{y}_i = (y_{i1}, y_{i2})^\top, \quad \mathbf{X}_i = \begin{pmatrix} 1 & x_{i1} & x_{i2} & 0 & 0 & 0 \\ 0 & 0 & 0 & 1 & x_{i1} & x_{i2} \end{pmatrix}, \quad \boldsymbol{\beta} = (\beta_1, \dots, \beta_6)^\top$$

for $k = 2$ and $s = 6$. In small area estimation, our aim is to predict θ_i for each area. Although many approaches have been proposed for efficiently predicting θ_i , we focus on the hierarchical Bayesian approach (e.g., Datta et al., 1999) in this paper.

Although the multivariate Fay-Herriot (FH) model has received relatively less attention than its univariate counterpart, several important theoretical and applied studies have been conducted. From a frequentist perspective, Benavent and Morales (2016) considered multivariate FH models with autoregressive covariance structures for the random-effect vectors and investigated their mean squared errors. Ito and Kubokawa (2021) studied empirical Bayes confidence regions for model (2.1). In the Bayesian framework, Porter et al. (2015) proposed multivariate spatial FH models that incorporate multivariate conditional autoregressive (MCAR) priors through a hierarchical Bayesian approach.

The determination of whether multivariate random effects are present remains a critical methodological challenge. As discussed in Section 1, substantial progress has been made in the univariate setting, where Bayesian shrinkage estimation methods for random effects based on global-local shrinkage priors have been extensively developed. In contrast, methodological advances for the multivariate case are still relatively scarce. Recently, Ghosh et al. (2022) extended global-local priors to the multivariate setting. Based on model (2.1), they modeled the random effect vector as

$$\mathbf{u}_i \sim \mathcal{N}_k(\mathbf{0}, \lambda_i^2 \boldsymbol{\Sigma}), \quad \lambda_i \sim \pi(\lambda_i), \quad \boldsymbol{\Sigma} \sim \pi(\boldsymbol{\Sigma}), \quad i = 1, \dots, m, \quad (2.2)$$

where λ_i is a local shrinkage parameter for area i , and $\boldsymbol{\Sigma}$ is a $k \times k$ covariance matrix. This prior is both simple in form and theoretically tractable, and the authors derived theoretical results on the concentration of the shrinkage factor. The approach performs well in most practical

settings. Nonetheless, the model of Ghosh et al. (2022) has two limitations. First, since each area is assigned a single local parameter λ_i , element-wise shrinkage within each area is not possible. Second, the model does not account for spatial dependence. Element-wise shrinkage is particularly important for capturing heterogeneity among observed variables within a given area. For instance, in a specific region, either median income or median rent may take extreme values relative to other areas. If such a region represents a hotspot, it is desirable that the model can appropriately shrink each component to accurately reflect the underlying pattern. To the best of our knowledge, element-wise shrinkage of random effect vectors has not yet been incorporated into multivariate small area models. To address these limitations, the next section proposes a hierarchical Bayesian model for multivariate small area estimation that achieves element-wise shrinkage of the random effect vectors \mathbf{u}_i while simultaneously incorporating spatial correlation.

3 Global-local priors based on sandwich-mixture covariance structure for multivariate spatial FH models

When spatial information is available for each area, predictive accuracy can be further improved by accounting not only for correlations among variables but also for spatial dependence. In this section, we extend the multivariate small area model introduced in the previous section by incorporating spatial correlation, and propose a novel model that allows for flexible, element-wise shrinkage of the random effects.

3.1 The proposed methods

Following Gelfand and Vounatsou (2003), the proper multivariate conditional autoregressive (MCAR) prior is defined as

$$\mathbf{u} \sim \mathcal{N}_{mk}(\mathbf{0}, (\mathbf{D} - \rho \mathbf{W})^{-1} \otimes \Sigma), \quad (3.1)$$

where $(\mathbf{D} - \rho \mathbf{W})^{-1}$ is a $m \times m$ matrix, Σ is a $k \times k$ matrix, \mathbf{W} is an $m \times m$ adjacency matrix whose (i, j) -th element is w_{ij} , \mathbf{D} is a diagonal matrix with the diagonal elements being the

row sums of W , and $\rho \in [0, 1]$ is a spatial dependence parameter. Under this setting, the prior distribution (3.1) becomes proper. Assuming the prior (3.1) for random effects, Porter et al. (2015) and Wang et al. (2025) considered spatial small area estimation via the multivariate Fay-Herriot model:

$$\begin{aligned} \mathbf{y}_i &= \boldsymbol{\theta}_i + \boldsymbol{\varepsilon}_i, \quad \boldsymbol{\theta}_i = \mathbf{X}_i \boldsymbol{\beta} + \mathbf{u}_i, \quad \boldsymbol{\varepsilon}_i \sim \mathcal{N}_k(\mathbf{0}, \mathbf{V}_i), \quad \pi(\boldsymbol{\beta}) = 1, \\ \mathbf{u} &\sim \mathcal{N}_{mk}(\mathbf{0}, (\mathbf{D} - \rho \mathbf{W})^{-1} \otimes \boldsymbol{\Sigma}), \quad \boldsymbol{\Sigma} \sim \pi(\boldsymbol{\Sigma}), \quad \rho \sim \pi(\rho), \quad i = 1, \dots, m, \end{aligned} \quad (3.2)$$

where \mathbf{u} is a $mk \times 1$ vector of spatial random effect, which follows a separable multivariate CAR (MCAR) distribution (Carlin and Banerjee, 2003; Gelfand and Vounatsou, 2003). $\boldsymbol{\Sigma}$ is the $k \times k$ correlation matrix. This model is called separable because the correlation across variables is decoupled from the spatial covariance. The parameter $\rho \in [0, 1]$ controls the strength of spatial dependence. If $\rho = 0$, $\mathbf{u}_1, \dots, \mathbf{u}_m$ are independent. When $\rho = 0$ and $\mathbf{D} = \mathbf{I}_m$, the model (3.2) corresponds to the usual multivariate FH model. Moreover, when $\rho = 1$, the model reduces to the intrinsic MCAR model (Mardia, 1988), which corresponds to an improper prior distribution. Although the resulting posterior distribution may still be proper and can therefore be used for posterior inference, model comparison becomes difficult under an improper prior. For this reason, we adopt a proper MCAR prior in this study. In particular, model comparison in Section 5 is conducted using the Deviance Information Criterion (DIC).

As a prior distribution for \mathbf{u} in (3.2), we propose the following prior distribution for \mathbf{u} :

$$\begin{aligned} \mathbf{u} \mid \boldsymbol{\Sigma}, \boldsymbol{\Lambda}, \rho, \tau &\sim \mathcal{N}_{mk}(\mathbf{0}, \tau^2 \boldsymbol{\Lambda} ((\mathbf{D} - \rho \mathbf{W})^{-1} \otimes \boldsymbol{\Sigma}) \boldsymbol{\Lambda}), \\ \boldsymbol{\lambda}_i = (\lambda_{i1}, \dots, \lambda_{ik})^\top &\sim \prod_{j=1}^k \pi(\lambda_{i,j}), \quad i = 1, \dots, m, \\ \tau &\sim \pi(\tau), \end{aligned} \quad (3.3)$$

where $\boldsymbol{\Lambda} = \text{blockdiag}(\boldsymbol{\Lambda}_1, \dots, \boldsymbol{\Lambda}_m) \in \mathbb{R}^{mk \times mk}$ with $\boldsymbol{\Lambda}_i = \text{diag}(\lambda_{i1}, \dots, \lambda_{ik})$. Following Hamura et al. (2025), we call the prior (3.3) *sandwich mixture prior*. Such sandwich-type covariance matrices have recently been employed in various models. For instance, Tang and Ghosh (2023) utilized them in univariate spatial small area estimation, while Hamura et al. (2025) applied them in multivariate robust Bayesian inference.

From the formulation

$$\mathbf{y} | \boldsymbol{\theta} \sim \mathcal{N}_{mk}(\boldsymbol{\theta}, \mathbf{V}), \quad \boldsymbol{\theta} | \boldsymbol{\beta}, \Sigma, \Lambda, \rho, \tau \sim \mathcal{N}_{mk}(\mathbf{X}\boldsymbol{\beta}, \tau^2 \Lambda ((\mathbf{D} - \rho \mathbf{W})^{-1} \otimes \Sigma) \Lambda),$$

the conditional posterior mean of the small area mean vector is given by

$$E(\boldsymbol{\theta} | \boldsymbol{\beta}, \Sigma, \Lambda, \rho, \tau, \mathbf{y}) = (\mathbf{I}_{mk} - \mathbf{Q})\mathbf{y} + \mathbf{Q}\mathbf{X}\boldsymbol{\beta},$$

where $\mathbf{Q} = (\mathbf{V}^{-1} + \mathbf{U}^{-1})^{-1}\mathbf{U}^{-1}$ and $\mathbf{U} = \tau^2 \Lambda ((\mathbf{D} - \rho \mathbf{W})^{-1} \otimes \Sigma) \Lambda$. The matrix \mathbf{Q} is called the matrix shrinkage factor. Since the matrix shrinkage factor \mathbf{Q} is not a diagonal matrix unlike theta in the Fay-Herriot model, the interpretation tends to be difficult. In contrast to the prior distribution defined in equation (2.2), the sandwich-type prior poses theoretical challenges for analyzing the posterior distribution of the shrinkage factor matrix. Following previous studies (e.g., Ghosh et al., 2022; Tang and Ghosh, 2023), we also assume $\pi(\boldsymbol{\beta}) \propto 1$.

Proposition 3.1 (Posterior propriety). *Under the prior distribution (3.3), if the priors of Σ , $\rho \in (0, 1)$, τ and λ_{ij} are proper, then the posterior density is proper.*

The proof is given in Appendix A.

3.2 Prior specification

We assume that $\Sigma \sim \text{IW}(\nu_0, \mathbf{B})$ for fixed hyper-parameters ν_0 and \mathbf{B} , where $\text{IW}(\nu, \mathbf{S})$ is the inverse Wishart distribution with degrees of freedom ν and covariance matrix \mathbf{B} . We employ $\nu = k$ and $\mathbf{B} = \mathbf{I}_k$ as default values of these hyper-parameters. Also, we assume the discrete uniform prior for ρ . Following Gelfand and Vounatsou (2003), we put equal mass on the following 31 values: 0, 0.05, 0.1, . . . , 0.8, 0.82, 0.84, . . . , 0.90, 0.91, 0.92, . . . , 0.99. The selection of a prior for local parameters is crucial for global-local shrinkage estimation of \mathbf{u}_i . In the literature, prior distributions for local shrinkage parameter can be divided into two groups, one with exponential tails and the other with polynomial tails. We consider two priors for global and local parameters.

- (Normal-gamma prior): If $\tau^2 = 1$ and $\pi(\lambda_{i,j}) = \frac{2b^a}{\Gamma(a)} \lambda_{i,j}^{2a-1} \exp(-b\lambda_{i,j}^2)$, the corresponding prior is called normal-gamma prior (Griffin and Brown, 2010; Tang and Zhang, 2024).

When $a = 1$, $\lambda_{i,j}^2$ follows the exponential distribution (see also, Park and Casella, 2008).

As the parameter a approaches zero, the contraction effect in the neighborhood of the origin becomes increasingly significant.

- (Horseshoe prior): If $\pi(\lambda_{i,j}) = (2/\pi)(1 + \lambda_{i,j}^2)^{-1}$, where $C_+(0, 1)$ denotes the standard half-Cauchy distribution and $\tau \sim C_+(0, 1)$, the corresponding prior is called horseshoe prior (Carvalho et al., 2010). Compared to the normal-gamma prior, the horseshoe prior provides markedly more aggressive shrinkage in the vicinity of zero, yet remains robust in that it applies minimal shrinkage to large signals.

Under the prior distribution (3.3), the marginal prior density of \mathbf{u} evaluated at $\mathbf{0}$, after integrating out $\boldsymbol{\lambda}$, is given by

$$\begin{aligned}\pi(\mathbf{u} = \mathbf{0}) &= C_1 \int |\tau^2 \boldsymbol{\Lambda}((\mathbf{D} - \rho \mathbf{W})^{-1} \otimes \boldsymbol{\Sigma}) \boldsymbol{\Lambda}|^{-1/2} \prod_{i=1}^m \prod_{j=1}^k \pi(\lambda_{i,j}) d\boldsymbol{\lambda} \\ &= C_2 \int |\boldsymbol{\Lambda}|^{-1} \prod_{i=1}^m \prod_{j=1}^k \pi(\lambda_{i,j}) d\boldsymbol{\lambda} = C_2 \int \prod_{i=1}^m \prod_{j=1}^k \lambda_{i,j}^{-1} \pi(\lambda_{i,j}) d\lambda_{i,j},\end{aligned}$$

where C_1 and C_2 denote constants that do not depend on $\boldsymbol{\lambda}$. If $\lambda_{i,j} \sim C_+(0, 1)$, that is, a standard half-Cauchy distribution, the above integral diverges to infinity. This implies that the marginal prior density of \mathbf{u} under the half-Cauchy prior has a pole at $\mathbf{u} = \mathbf{0}$, thereby inducing strong shrinkage toward zero. The normal-gamma prior does not induce shrinkage as aggressively as the horseshoe prior, and its tails are comparatively lighter. However, it is expected to perform well when the underlying sparsity is moderate. Therefore, in this paper, we employ both of these priors as prior distributions for the local parameters. Although various other types of shrinkage priors exist and they are also conceptually applicable, it has been empirically observed that they tend to exhibit broadly similar performance in practical applications (e.g., Ghosh et al., 2022).

3.3 Posterior computation

We present an MCMC algorithm for posterior computation. The random effect vector \mathbf{u} can be expressed as

$$\mathbf{u} = \boldsymbol{\Lambda} \tilde{\mathbf{u}}, \quad \tilde{\mathbf{u}} \sim \mathcal{N}_{mk}(\mathbf{0}, \tau^2((\mathbf{D} - \rho \mathbf{W})^{-1} \otimes \boldsymbol{\Sigma})). \quad (3.4)$$

Furthermore, from the definition of the proper MCAR model, we note that the full conditional prior distribution of $\tilde{\mathbf{u}}_i$ is given by

$$\tilde{\mathbf{u}}_i \mid \{\tilde{\mathbf{u}}_j\}_{j \neq i} \sim \mathcal{N}_k \left(\rho \sum_{j \sim i} \frac{1}{w_{i+}} \tilde{\mathbf{u}}_j, \frac{\tau^2}{w_{i+}} \Sigma \right), \quad (3.5)$$

where $w_{i+} = \sum_{j=1}^m w_{ij}$.

The joint posterior density is proportional to

$$\begin{aligned} \pi(\tilde{\mathbf{u}}, \boldsymbol{\beta}, \Sigma, \Lambda, \rho, \tau^2 \mid \mathbf{y}) &\propto \exp \left[-\frac{1}{2} (\mathbf{y} - \mathbf{X}\boldsymbol{\beta} - \Lambda \tilde{\mathbf{u}})^\top \mathbf{V}^{-1} (\mathbf{y} - \mathbf{X}\boldsymbol{\beta} - \Lambda \tilde{\mathbf{u}}) \right] \\ &\quad \times |\tau^2((\mathbf{D} - \rho \mathbf{W})^{-1} \otimes \Sigma)|^{-1/2} \exp \left[-\frac{1}{2} \tilde{\mathbf{u}}^\top \frac{1}{\tau^2} ((\mathbf{D} - \rho \mathbf{W}) \otimes \Sigma^{-1}) \tilde{\mathbf{u}} \right] \\ &\quad \times |\Sigma|^{-(\nu_0 + k + 1)/2} \exp\{-\text{tr}(\mathbf{B}\Sigma^{-1})/2\} \left(\prod_{i=1}^m \prod_{j=1}^k \pi(\lambda_{i,j}) \right) \pi(\rho) \pi(\tau^2), \end{aligned}$$

where we set $\pi(\tau^2) = \delta_1$ where δ_1 denotes a point mass at 1 and $\pi(\lambda_{i,j}) = \pi(\lambda_{i,j} \mid a, b) \pi(a) \pi(b)$ for the normal-gamma prior.

Under prior distributions presented in Section 3.2, we summarize the MCMC algorithm as follows. The derivations are provided in Appendix B.1.

- Draw $\boldsymbol{\beta}$ from $\mathcal{N}_s(\mathbf{m}, (\mathbf{X}^\top \mathbf{V}^{-1} \mathbf{X})^{-1})$, where $\mathbf{m} = (\mathbf{X}^\top \mathbf{V}^{-1} \mathbf{X})^{-1} \mathbf{X}^\top \mathbf{V}^{-1} \mathbf{z}$, $\mathbf{z} := \mathbf{y} - \Lambda \tilde{\mathbf{u}}$ and $\mathbf{V} = \text{blockdiag}(\mathbf{V}_1, \dots, \mathbf{V}_m) \in \mathbb{R}^{mk \times mk}$.
- Draw $\tilde{\mathbf{u}}_i$ from $\mathcal{N}_k(\mathbf{A}^{-1} \mathbf{b}, \mathbf{A}^{-1})$, where $\mathbf{A} = \Lambda_i \mathbf{V}_i^{-1} \Lambda_i + \Omega_{\text{CAR},i}^{-1}$ and $\mathbf{b} = \Lambda_i \mathbf{V}_i^{-1} \boldsymbol{\xi}_i + \Omega_{\text{CAR},i}^{-1} \boldsymbol{\mu}_{\text{CAR},i}$ with $\boldsymbol{\mu}_{\text{CAR},i} = \rho \sum_{j \sim i} \frac{1}{w_{i+}} \tilde{\mathbf{u}}_j$, $\Omega_{\text{CAR},i} = \frac{\tau^2}{w_{i+}} \Sigma$, and $\boldsymbol{\xi}_i = \mathbf{y}_i - \mathbf{X}_i \boldsymbol{\beta}$.
- Draw Σ from $\text{IW}(m + \nu_0, \mathbf{B} + \tau^{-2} \tilde{\mathbf{U}} (\mathbf{D} - \rho \mathbf{W}) \tilde{\mathbf{U}}^\top)$, where $\tilde{\mathbf{U}} := (\tilde{\mathbf{u}}_1, \dots, \tilde{\mathbf{u}}_m) \in \mathbb{R}^{k \times m}$.
- Draw ρ using the full conditional distribution

$$\pi(\rho \mid -) \propto |\mathbf{D} - \rho \mathbf{W}|^{k/2} \times \exp \left[-\frac{1}{2} \tau^{-2} \tilde{\mathbf{u}}^\top ((\mathbf{D} - \rho \mathbf{W}) \otimes \Sigma^{-1}) \tilde{\mathbf{u}} \right].$$

- Draw $\boldsymbol{\lambda}_i$ using the full conditional distribution

$$\pi(\boldsymbol{\lambda}_i | -) \propto \exp \left[-\frac{1}{2} \left(\frac{\mathbf{y}_i - \mathbf{X}_i \boldsymbol{\beta}}{\tilde{\mathbf{u}}_i} - \boldsymbol{\lambda}_i \right)^\top \tilde{\mathbf{U}}_i \mathbf{V}_i^{-1} \tilde{\mathbf{U}}_i \left(\frac{\mathbf{y}_i - \mathbf{X}_i \boldsymbol{\beta}}{\tilde{\mathbf{u}}_i} - \boldsymbol{\lambda}_i \right) \right] \prod_{j=1}^k \pi(\lambda_{i,j}), \quad (3.6)$$

where the fraction $\frac{\mathbf{y}_i - \mathbf{X}_i \boldsymbol{\beta}}{\tilde{\mathbf{u}}_i}$ is taken elementwise and $\tilde{\mathbf{U}}_i = \text{diag}(\tilde{u}_{i1}, \dots, \tilde{u}_{ik})$.

- Sampling of τ^2 (horseshoe prior): Using

$$\tau \sim \text{C}_+(0, 1) \iff \tau^2 | \psi \sim \text{IG}(1/2, 1/\psi), \quad \psi \sim \text{IG}(1/2, 1),$$

sample τ^2 from $\text{IG}\left(\frac{mk+1}{2}, \frac{1}{2}\tilde{\mathbf{u}}^\top((\mathbf{D} - \rho\mathbf{W}) \otimes \boldsymbol{\Sigma}^{-1})\tilde{\mathbf{u}} + \frac{1}{\psi}\right)$ and sample ψ from $\text{IG}\left(\frac{1}{2}, \frac{1}{\tau^2} + 1\right)$

- Sampling of a and b (normal-gamma prior): Under the prior $a \sim U(0, 1)$ and $b \sim \text{Ga}(c, d)$, sample $b \sim \text{Ga}\left(amk + c, \sum_{i=1}^m \sum_{j=1}^k \lambda_{i,j}^2 + d\right)$ and sample a using the full conditional distribution

$$\pi(a | -) \propto \prod_{i=1}^m \prod_{j=1}^k \frac{b^a}{\Gamma(a)} \lambda_{i,j}^{2a-1} = \left(\frac{b^a}{\Gamma(a)} \right)^{mk} \left(\prod_{i=1}^m \prod_{j=1}^k \lambda_{i,j} \right)^{2a-1}.$$

The first term on the right-hand side of (3.6) is proportional to the normal density but with the constraint $\boldsymbol{\lambda}_i > \mathbf{0}$, that is, $\lambda_{ij} > 0$ for all j . Following Tang and Ghosh (2023), we employ constraint relaxation by approximating the indicator function $\prod_{j=1}^k 1_{(0,\infty)}(\lambda_{ij})$ by a sigmoid function $\prod_{j=1}^k 1/(1 + \exp(-\eta\lambda_{ij}))$ for a large constant $\eta > 0$ (see also, Ray et al., 2020; Onizuka et al., 2024). Then we use the elliptical slice sampler (Murray et al., 2010; Hahn et al., 2019) to draw samples for $\boldsymbol{\lambda}_i$. The details of the sampling method are provided in Appendix B.2. Since the full conditional distributions of ρ and of a (used in the normal-gamma prior) do not correspond to any standard probability distributions, we employ grid-based sampling for each of them in this study. Furthermore, to reduce the computational burden in sampling ρ , we define $\mathbf{S} = \mathbf{D}^{-1/2} \mathbf{W} \mathbf{D}^{-1/2}$ and use the identity

$$|\mathbf{D} - \rho\mathbf{W}| = |\mathbf{D}| |\mathbf{I}_m - \rho\mathbf{S}| = |\mathbf{D}| \prod_{i=1}^m (1 - \rho\gamma_i),$$

where γ_i denotes the eigenvalues of \mathbf{S} . Note that these eigenvalues need to be computed only once.

3.4 Non-Gaussian response

The proposed methods can be extended to some non-Gaussian responses such as binomial and Poisson responses. The binomial distribution is frequently employed to model proportions such as disease prevalence or poverty rates, while the Poisson distribution is commonly used to model the number of cases in a given area. The latter is particularly useful in applied contexts and is often referred to as disease mapping (e.g., MacNab, 2022). Although we do not explore the details in this paper, it is worth noting that the computational complexity increases when moving from the normal distribution to the Poisson case. In fact, it is well known that posterior inference for spatial regression models based on the Poisson likelihood is computationally demanding. On the other hand, by approximating the Poisson model with a negative binomial distribution, it becomes feasible to leverage Pólya-Gamma data augmentation techniques (Polson et al., 2013), in a manner analogous to the binomial case.

4 Simulation

We conduct simulation studies to illustrate the performance of the proposed methods.

4.1 Setting

We investigate the performance of different priors for estimating the small area means on simulated datasets. We generate data from the model:

$$\mathbf{y}_i = \mathbf{X}_i \boldsymbol{\beta} + \mathbf{u}_i + \boldsymbol{\varepsilon}_i, \quad \boldsymbol{\varepsilon}_i \sim \mathcal{N}_k(\mathbf{0}, \mathbf{V}_i), \quad i = 1, \dots, m,$$

where $\boldsymbol{\beta} = (1, 1, 1, 1)^\top$, $\mathbf{x}_i = (1, x_{i,1})^\top$, where $x_{i,1}$ is generated from the standard normal distribution. We consider the bivariate case ($k = 2$) and $m = 100, 200$ and 500 . Concerning the dispersion matrices \mathbf{V}_i of sampling errors $\boldsymbol{\varepsilon}$, we consider two cases: (a) $0.7\mathbf{I}_k, 0.6\mathbf{I}_k, 0.5\mathbf{I}_k, 0.4\mathbf{I}_k, 0.3\mathbf{I}_k$; (b) $2.0\mathbf{I}_k, 0.6\mathbf{I}_k, 0.5\mathbf{I}_k, 0.4\mathbf{I}_k, 0.2\mathbf{I}_k$ (see also Datta et al., 2005; Ito and Kubokawa, 2020). These error covariances are randomly assigned to each area in equal proportions. In the

observation-error covariance matrix, the correlations are set to zero, although a more general treatment is possible. In practice, however, direct estimates of correlation coefficients between observations are seldom available, as in the real-world dataset analyzed in Section 5. For this reason, and for simplicity, we assume zero correlation.

To model spatial dependence, we constructed an adjacency matrix \mathbf{W} based on a regular lattice structure. Specifically, we considered a rectangular $10 \times (m/10)$ grid where each cell corresponds to a spatial unit. Two units are considered adjacent (i.e., $w_{ij} = 1$) if they share a common edge (i.e., they are first-order neighbors in the cardinal directions: up, down, left, or right). Diagonal adjacency is not considered. The resulting matrix \mathbf{W} is symmetric and binary, with $w_{ij} = 1$ indicating adjacency and $w_{ij} = 0$ otherwise.

For generating a true random effect vector $\mathbf{u} \in \mathbb{R}^{mk}$, we consider the following cases. For all scenarios, we set $\rho = 0.95$ and Σ is the correlation matrix with correlation coefficient 0.3.

- **(Scenario 1):** Let $\mathbf{u} \sim \mathcal{N}_{mk}(\mathbf{0}, (\mathbf{D} - \rho\mathbf{W})^{-1} \otimes \Sigma)$.
- **(Scenario 2):** Let $\mathbf{u} \sim \mathcal{N}_{mk}(\boldsymbol{\mu}, (\mathbf{D} - \rho\mathbf{W})^{-1} \otimes \Sigma)$, where each component of $\boldsymbol{\mu}$ is generated from $(1 - z)\delta_5 + z\delta_0$, with $z \sim \text{Ber}(\omega)$ and δ_x denoting a point mass at x . We set $\omega = 0.5$.
- **(Scenario 3):** The same as Scenario 2, except that we set $\omega = 0.8$.
- **(Scenario 4):** Let $\mathbf{u} \sim \mathcal{N}_{mk}(\mathbf{0}, 4((\mathbf{D} - \rho\mathbf{W})^{-1} \otimes \Sigma))$. For each variable (i.e., for the vectors $(u_{1,1}, \dots, u_{m,1})$ and $(u_{1,2}, \dots, u_{m,2})$), the lower 50% of the elements in terms of absolute magnitude are replaced with zero.
- **(Scenario 5):** Let $\mathbf{u} \sim \mathcal{N}_{mk}(\mathbf{0}, 4((\mathbf{D} - \rho\mathbf{W})^{-1} \otimes \Sigma))$. For each variable, the lower 80% of the elements in terms of absolute magnitude are replaced with zero.

Scenario 1 assumes a Gaussian distribution for the random effects, which is the standard specification commonly used in spatial Fay–Herriot (FH) models. In Scenarios 2 and 3, the random effects follow a two-component mixture distribution that represents a combination of signal and noise: values equal to 0 correspond to noise, while those equal to $\mu = 5$ represent nonzero signal. The choice $\mu = 5$ ensures that the signal is sufficiently distinguishable from noise, as

smaller values may lead to weak identifiability. The sparsity level of the non-signal components is controlled by ω . Specifically, $\omega = 0.5$ (Scenario 2) represents a setting in which signal and noise are present in equal proportions, whereas $\omega = 0.8$ (Scenario 3) corresponds to a setting in which the proportion of signal is smaller. These scenarios are commonly used when evaluating the performance of shrinkage priors. Scenarios 4 and 5 introduce an alternative form of sparsity that is generated directly from Gaussian random effects (see also Tang and Ghosh, 2023). After drawing \mathbf{u} from a spatially correlated normal distribution with inflated variance, we enforce sparsity by thresholding: for each variable, the lower 50% (Scenario 4) or 80% (Scenario 5) of the components in terms of absolute magnitude are set to zero. These scenarios differ from Scenarios 2 and 3 in that sparsity arises from magnitude-based thresholding rather than a discrete mixture distribution, and in that some random effects are replaced with exactly zero, thereby allowing us to assess the robustness of the methods against different forms of sparsity.

We compare the following five methods: (I) The proposed model under the horseshoe prior (3.3) (denoted by **SpaHS**); (II) The proposed model under the normal-gamma prior (3.3) (denoted by **SpaGa**) (III) The multivariate spatial FH model (3.2) (denoted by **SpaFH**); (IV) the multivariate global-local model under the horseshoe prior (2.2) proposed by Ghosh et al. (2022) (denoted by **HS**); (V) the multivariate Fay-Herriot model (2.1) (denoted by **FH**). Note that we assume $a \sim \text{DiscreteUniform}(0.01, 0.02, \dots, 0.99, 1.0)$ and $b \sim \text{Ga}(0.001, 0.001)$ for the **SpaGa** method. For each of these models, we run MCMC for 2,000 iterations. The first 500 iterations are discarded as the burn-in period. The small area means θ_i are estimated by using the posterior means.

We evaluated the performance of estimation for θ using average absolute deviation (AAD) and average squared deviation (ASD), which are defined as follows:

$$\text{AAD} = \frac{1}{mk} \sum_{i=1}^m \sum_{j=1}^k |\hat{\theta}_{ij} - \theta_{ij}|, \quad \text{ASD} = \frac{1}{mk} \sum_{i=1}^m \sum_{j=1}^k (\hat{\theta}_{ij} - \theta_{ij})^2.$$

The empirical coverage rate (CP) and average length (AL) of 95% credible intervals of θ_{ij} are also used to evaluate the interval estimates. For a given situation, we report the median of the four measures over the 50 datasets.

4.2 Simulation results

First, we examine the behavior of the local parameters λ in the proposed method SpaHS and the existing method HS using a single simulation run. Here, we consider Scenario 5 with $m = 500$ and observation variance corresponding to case (a). Figure 1 displays the distribution of the true random effect vectors and the posterior means of the estimated local parameters under the two methods. Note that for SpaHS, the local parameters are given by $\boldsymbol{\lambda}^{\text{SpaHS}} = (\lambda_{1,1}, \lambda_{1,2}, \dots, \lambda_{500,1}, \lambda_{500,2})^\top$, whereas for HS they are given by $\boldsymbol{\lambda}^{\text{HS}} = (\lambda_1, \dots, \lambda_{500})^\top$. The left panel shows the true two-dimensional random effects $\mathbf{u}_i = (u_{i,1}, u_{i,2})^\top$ for each area, where the color indicates the number of nonzero components in \mathbf{u}_i . Specifically, points at the center correspond to $\mathbf{u}_i = \mathbf{0}$ (zero nonzero components), points lying on one of the axes correspond to cases where only one component of \mathbf{u}_i is nonzero (one nonzero component), and points off the axes correspond to cases where both components are nonzero (two nonzero components). From this panel, we observe substantial heterogeneity across areas in the magnitude of the random effects at the component level. The middle and right panels plot the posterior means of the local parameters for HS and SpaHS, respectively, using the same color coding as in the left panel. Since HS performs shrinkage jointly at the area level, the estimated local parameters tend to be uniformly small (red) or large (blue) within each area, while areas with only one nonzero component in \mathbf{u}_i (green) exhibit intermediate shrinkage. In contrast, SpaHS allows component-wise shrinkage: red points correspond to small values in both dimensions, blue points to large values in both dimensions, and green points are aligned along the axes, indicating that shrinkage is applied selectively to each component. These results demonstrate that, in such scenarios, the proposed SpaHS method is capable of more flexible and adaptive shrinkage compared with HS.

Next, we report the simulation results in Figures 2 and 3. Figure 2 corresponds to variance scenario (a), whereas Figure 3 pertains to scenario (b), where the area-specific variances exhibit greater variability. We first focus on the point estimation results shown in the top two rows of each figure. In Scenario 1, the SpaFH model performs well across all configurations, which is expected since the data-generating mechanism follows the SpaFH specification. SpaGa achieves the second-best performance in this scenario. This is reasonable since the current version of SpaGa, although less capable of extreme shrinkage than the horseshoe prior, can adapt-

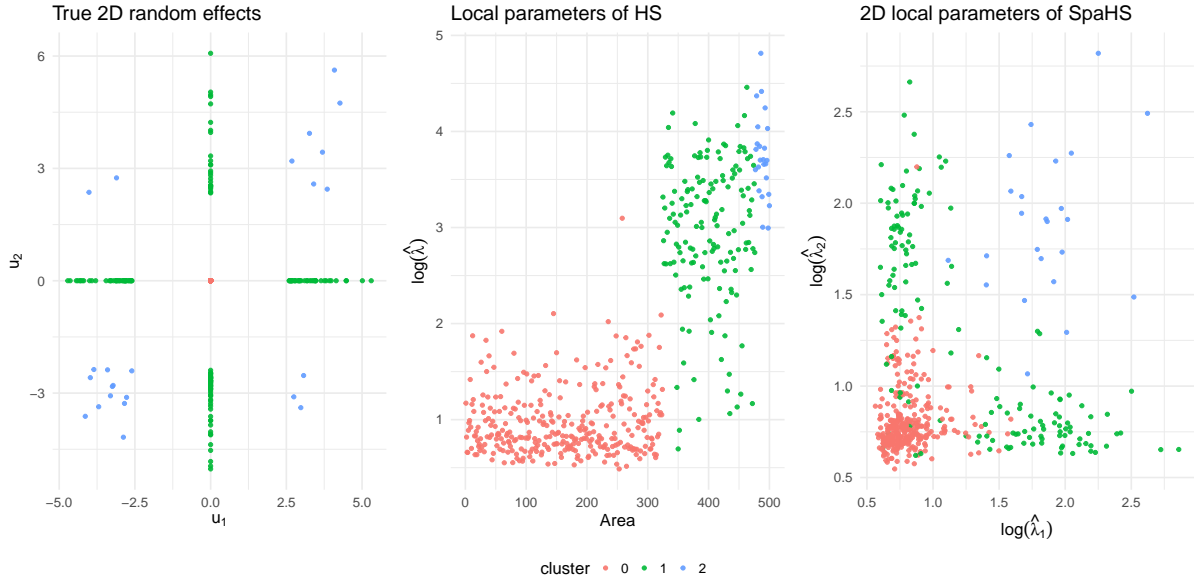


Figure 1: Results from a single simulation run for true random effects (left) and posterior mean estimates of the local parameters under HS (center) and SpaHS (right) for Scenario 5 with $m = 500$ and observation variance case (a). For HS, each area has a single local parameter, and thus the x -axis represents the area index. In contrast, SpaHS assigns two local parameters to each area, which are plotted in two dimensions.

tively control the amount of shrinkage through the parameter a , which is estimated from the data via MCMC. Under Scenario 2, SpaHS and SpaGa perform similarly. In particular, when the sampling error covariance exhibits high area-to-area variability (scenario (b)), SpaHS and SpaGa yield almost identical ASD values, and even the standard FH model without spatial effects performs reasonably well. In Scenario 3, SpaHS provides the best performance due to the horseshoe prior, which is well suited for sparse structures. In contrast, SpaGa performs slightly worse under these conditions, and the HS model proposed by Ghosh et al. (2022), which incorporates neither spatial dependence nor element-wise shrinkage, performs comparably to SpaGa.

In the thresholded sparsity scenarios (Scenarios 4 and 5), SpaHS again performs consistently well. When the proportion of nonzero elements is 50% (Scenario 4), SpaFH also yields good results. Notably, SpaGa – which performs well in Scenarios 2 and 3 – shows a clear deterioration in Scenarios 4 and 5. This decline is likely due to the nature of the normal-gamma prior, which induces partial shrinkage toward zero and is therefore less suited to thresholded sparsity structures.

The bottom two rows of Figures 2 and 3 summarize the uncertainty quantification results. Although differences across methods are generally small, SpaHS yields shorter credible inter-

vals and coverage probabilities closer to the nominal 95% level in many scenarios. In Scenarios 4 and 5, where SpaGa performs poorly in terms of point estimation, its credible intervals also noticeably underperform relative to the other methods.

Overall, SpaHS performs particularly well when the underlying signal is sparse. SpaGa also offers stable estimates in Scenarios 1 to 3. From a practical standpoint, one may consider applying both SpaHS and SpaGa models and selecting between them using an appropriate model comparison criterion. We experimented with three different numbers of areas, $m = 100, 200$, and 500 , and the results were largely consistent across these settings. Because the proposed methods involve mk local parameters, repeated experiments for substantially larger m were not feasible due to computational constraints. Investigating the performance of these methods for larger m remains an interesting direction for future work.

5 Real data analysis

In the context of small area estimation, we analyze county-level data in the West Census Region using two key socioeconomic indicators: median household income and poverty rate. Many counties have unreliable direct estimates due to small sample sizes; thus, jointly modeling these two correlated variables allows us to borrow strength across indicators and improve estimation accuracy. Moreover, by incorporating spatial information, the model can leverage correlations among neighboring counties, capturing spatial dependencies and identifying areas exhibiting extreme values (hotspots) in income or poverty. This approach provides more reliable and nuanced estimates, which can inform policy decisions and targeted interventions in the region. As a key feature of the proposed method is its ability to accurately identify counties exhibiting extreme values in either income or poverty rate, while simultaneously improving the overall estimation precision across the region.

5.1 Dataset and setting

We use data from the 5-year American Community Survey (ACS) released in 2022, where the response variables are the estimated median household income and poverty rate, and the percentage of high school graduates is employed as an auxiliary covariate. We focus on the 413

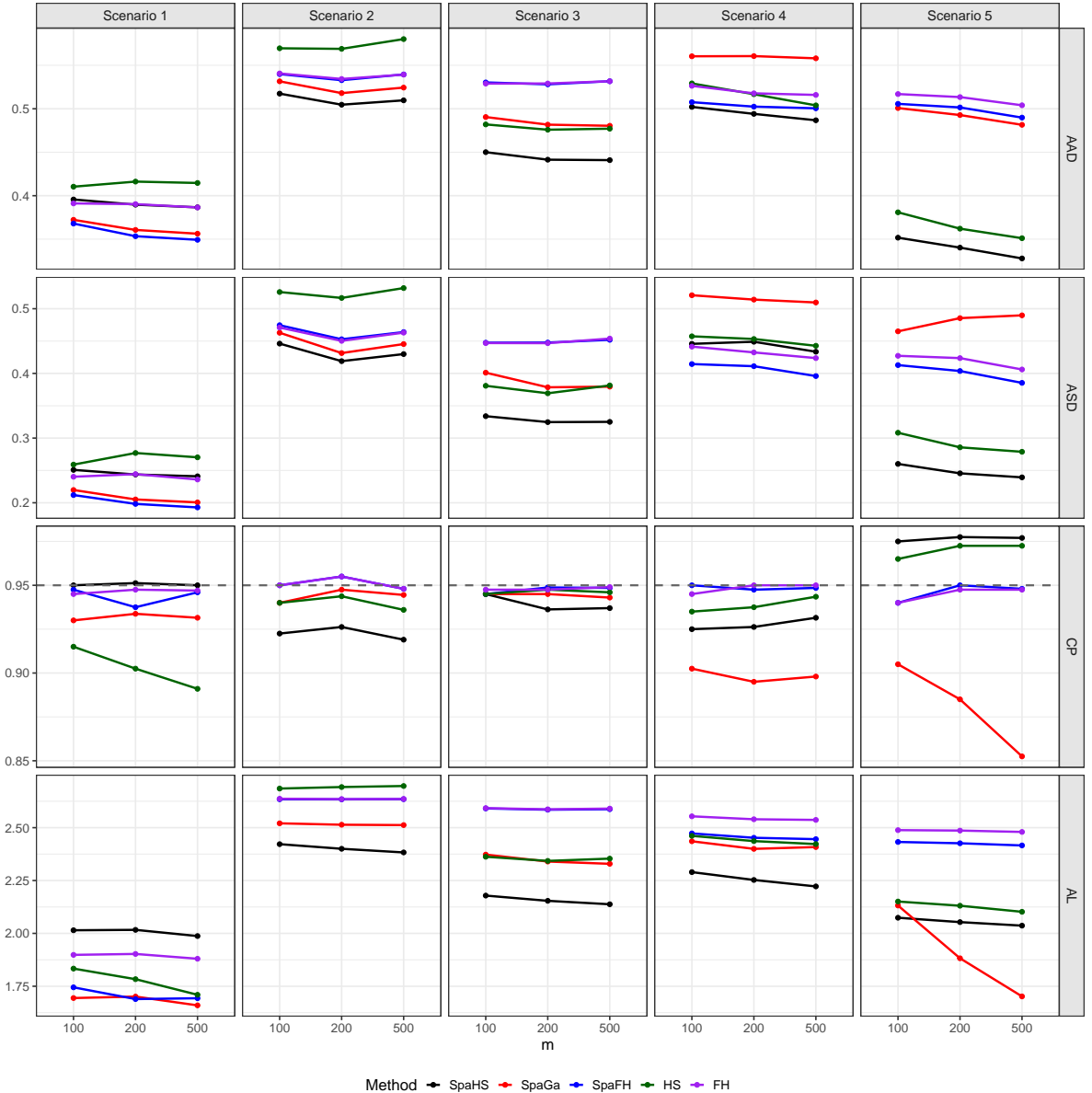


Figure 2: The average absolute deviation (AAD), average squared deviation (ASD), coverage probability of the 95% credible interval and average length of the 95% credible interval under the variance scenario (a). The figure displays the median computed over 50 replications and the horizontal axis is the number of small areas.

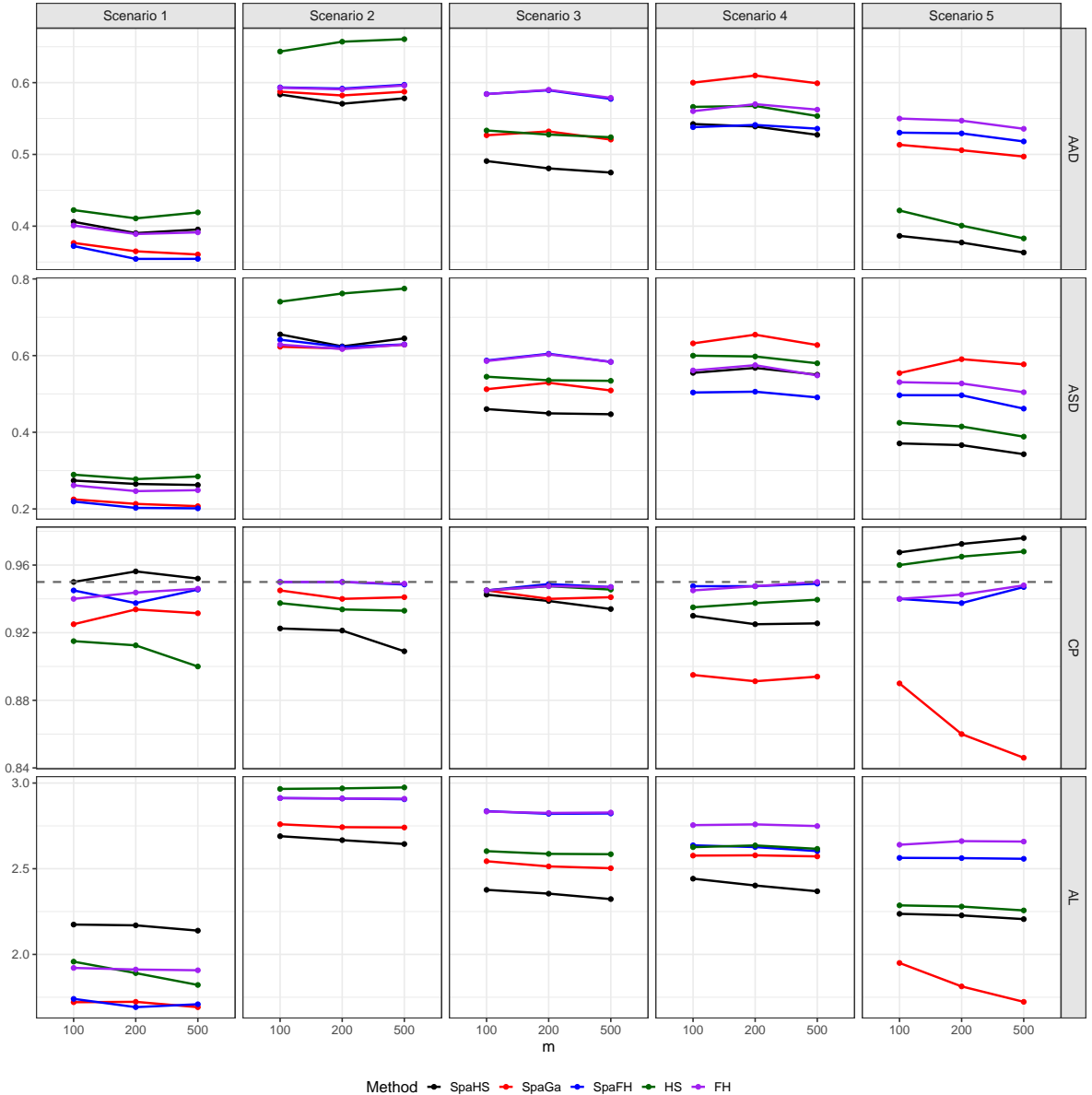


Figure 3: The average absolute deviation (AAD), average squared deviation (ASD), coverage probability of the 95% credible interval and average length of the 95% credible interval under the variance scenario (b). The figure displays the median computed over 50 replications and the horizontal axis is the number of small areas.

counties located in the West Census Region, excluding those that are geographic enclaves (non-contiguous counties). Tang et al. (2023) also analyzed poverty rates in the West Census Region. To better satisfy the normality assumption, the median household income and poverty rate were log-transformed, and the corresponding variances were computed using the Delta method. The variances of the log-transformed direct estimates are shown in Figure 4. The Moran's I statistics for the log-transformed direct estimates of the median household income and the poverty rate were 0.50 and 0.35, respectively (both with p -value < 0.001). These results indicate that both variables exhibit statistically significant positive spatial autocorrelation, suggesting the presence of spatial clustering rather than spatial randomness. In our study, we handle county-level data, and the sample sizes within each county are sufficiently large. Consequently, the variances of the direct estimates for most areas are relatively moderate. However, we observe that a few regions exhibit comparatively large variances. For example, with respect to median income, De Baca County, New Mexico and Esmeralda County, Nevada exhibit relatively high values of the sample variance. In terms of the poverty rate, Eureka County, Nevada and Camas County, Idaho likewise show notably elevated levels. Such counties tend to exhibit high levels of variance in socioeconomic indicators. This can be largely attributed to factors such as extremely small population sizes, the dominance of a limited number of industries, and the susceptibility of local statistics to substantial fluctuations resulting from minor demographic or economic changes. Additionally, survey-based estimates for such counties often involve relatively large sampling errors, further contributing to the observed variance. Since the ACS data do not provide covariance information between variables, we assume that the covariances among the direct estimates are zero.

The proposed SpaHS and SpaGa models, as well as the SpaFH model for comparison, are fitted to the data. The prior distributions for SpaHS, SpaGa, and SpaFH were set to be the same as those used in Section 4. For the HS and FH models, we employed the prior distributions specified by Ghosh et al. (2022). For each model, 20,000 MCMC iterations were performed, discarding the first 10,000 samples as burn-in. The adjacency matrix \mathbf{W} is constructed based on whether counties share a common border.

Model performance is evaluated using the Deviance Information Criterion (DIC). The DIC proposed by Spiegelhalter et al. (2002) is defined by $DIC = D(\bar{\boldsymbol{\theta}}) + 2p_D$, where $p_D = \bar{D} - D(\bar{\boldsymbol{\theta}})$

measures the model complexity, $D(\bar{\theta})$ is the deviance of the model evaluated at the posterior mean of model parameter θ , and \bar{D} is the posterior mean of the deviance. In our models, $D(\theta) = \sum_{i=1}^m (\mathbf{y}_i - \theta_i)^\top \mathbf{V}_i^{-1} (\mathbf{y}_i - \theta_i)$. Using a posterior sample $\theta^{(s)} = (\theta_1^{(s)}, \dots, \theta_m^{(s)})$ for $s = 1, \dots, S$, we obtain

$$\widehat{\text{DIC}} = \frac{2}{S} \sum_{s=1}^S \sum_{i=1}^m (\mathbf{y}_i - \theta_i^{(s)})^\top \mathbf{V}_i^{-1} (\mathbf{y}_i - \theta_i^{(s)}) - \sum_{i=1}^m (\mathbf{y}_i - \hat{\theta}_i)^\top \mathbf{V}_i^{-1} (\mathbf{y}_i - \hat{\theta}_i),$$

where $\hat{\theta}_i = (1/S) \sum_{s=1}^S \theta_i^{(s)}$ is the posterior sample mean of θ_i .

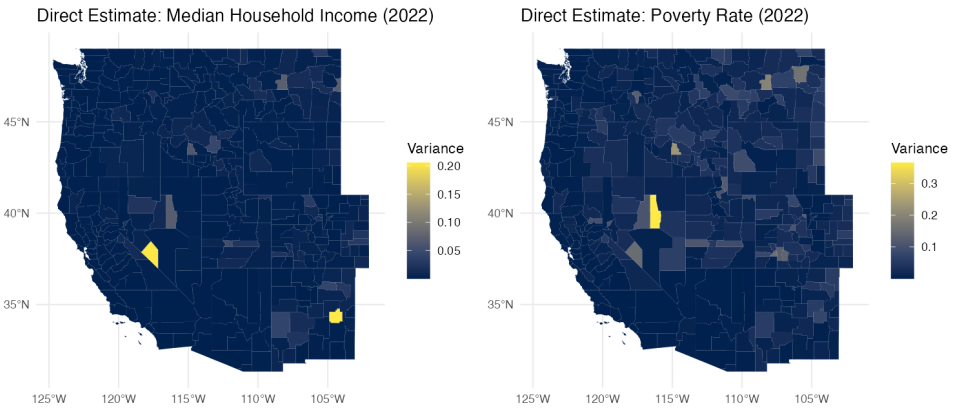


Figure 4: Variance on the log-scale of median household income and poverty rate of direct estimates for 413 counties in West Census Region, based on 5-year period estimates from the 2022 American Community Survey.

5.2 Results

Figure 5 presents the SpaHS estimates of income and poverty rates (posterior means of θ) alongside the corresponding estimates from SpaFH and SpaGa. Relative to SpaFH, the largest discrepancies appear in areas with lower outcome values, where SpaFH tends to slightly overestimate. In contrast, the SpaHS and SpaGa estimates of income are generally similar, while noticeable differences emerge for the poverty rate due to different levels of shrinkage applied by the models.

Figure 6 shows spatial maps of the SpaHS estimates of θ together with the corresponding direct estimates \mathbf{y}_i . Visual differences in the income estimates are modest. For the poverty rate,

however, the largest deviations between the SpaHS small-area means and the direct estimates occur in Petroleum County and Toole County, Montana, located in the northeastern portion of Figure 6. This pattern is consistent with the estimated random effects (posterior means of \boldsymbol{u}) shown in Figure 7, which suggest that the random effects exhibit a certain degree of sparsity. Several regions display high or low values (hot or cold spots). The variance of the random effects is larger for the poverty rate than for median income, and the largest posterior mean of SpaHS for the poverty rate is found in Morgan County, Utah, followed by Madison County, Idaho. Both counties show negative random effects and may be considered cold spots.

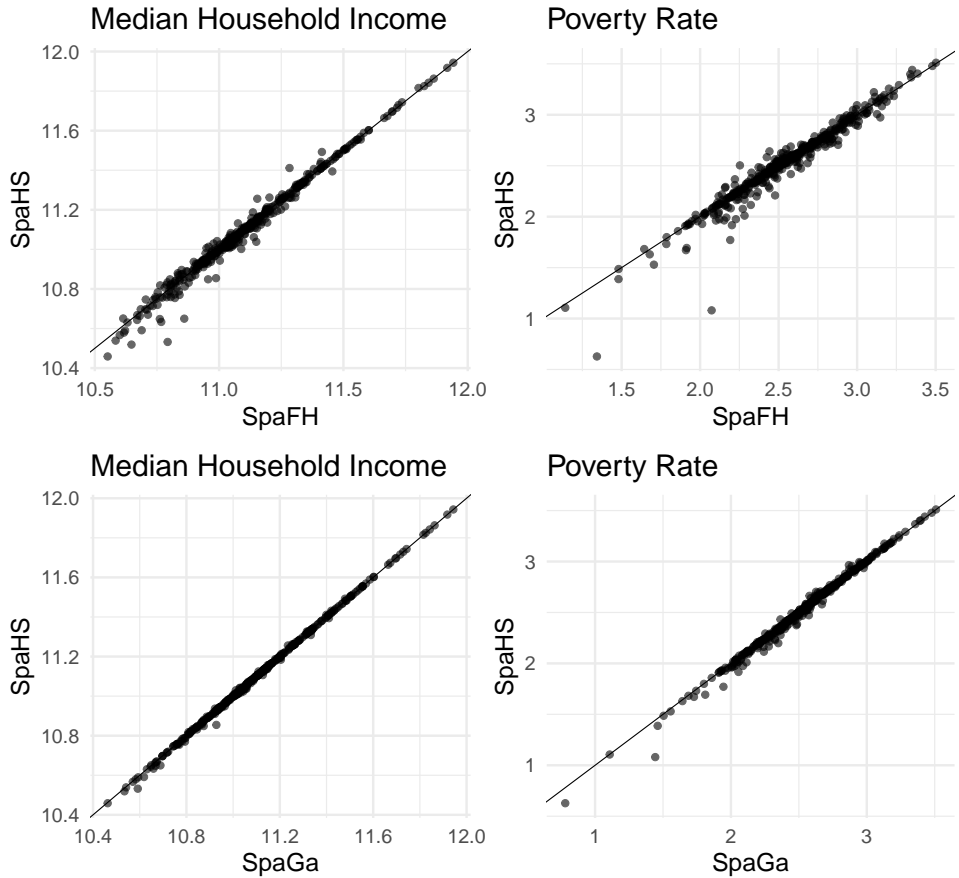


Figure 5: Posterior means of small area mean θ_i for the SpaHS, SpaGa and SpaFH methods.

Although these visualizations offer useful insights into the behavior of the models, they do not directly determine which model performs best. Model evaluation based on the DIC values in Table 1 shows that SpaHS provides the best overall fit, followed by SpaGa. The HS method of (Ghosh et al., 2022) performs less favorably for these data because it does not incorporate spatial dependence and cannot perform element-wise shrinkage. Table 1 also reports the mean effective sample size across the components of $\boldsymbol{\theta}$. Because this value is close to the total num-

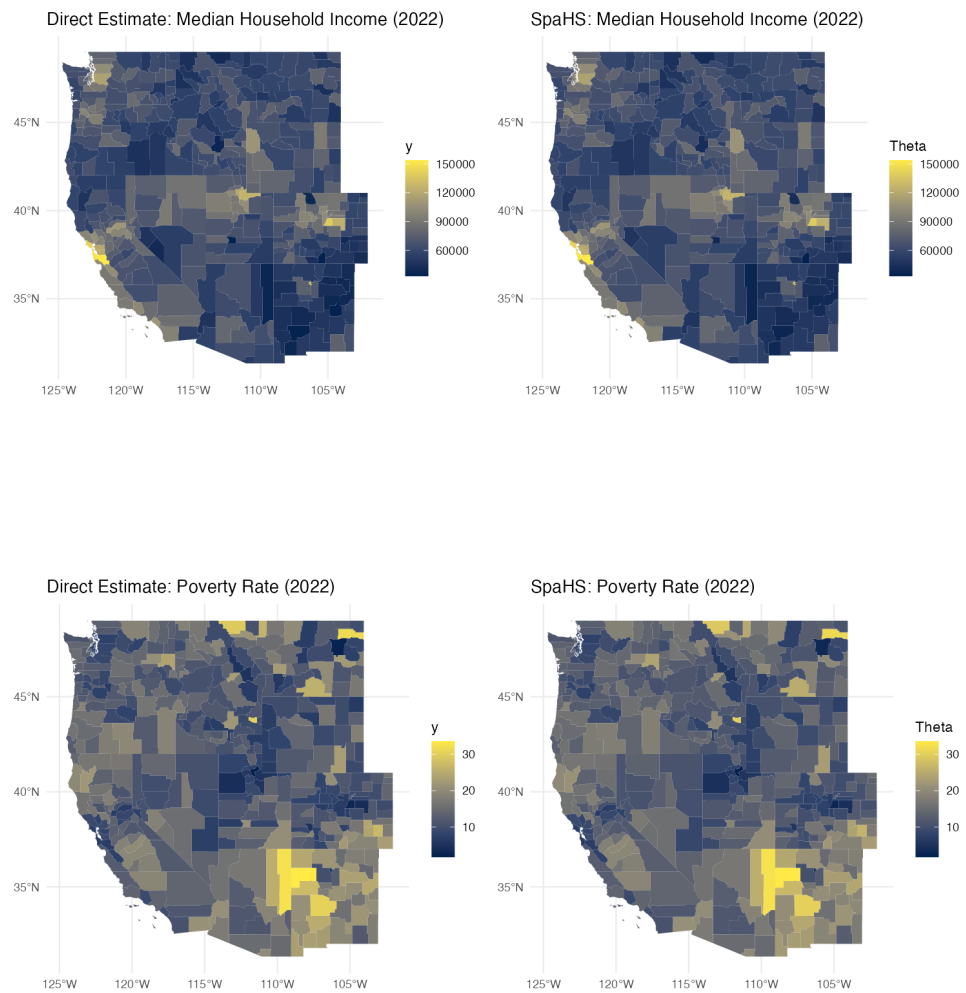


Figure 6: Estimates of median household income and poverty rate for 413 counties in West Census Region, based on 5-year period estimates from the 2022 American Community Survey, including direct estimates and results from the SpaHS, SpaGa and SpaFH methods.

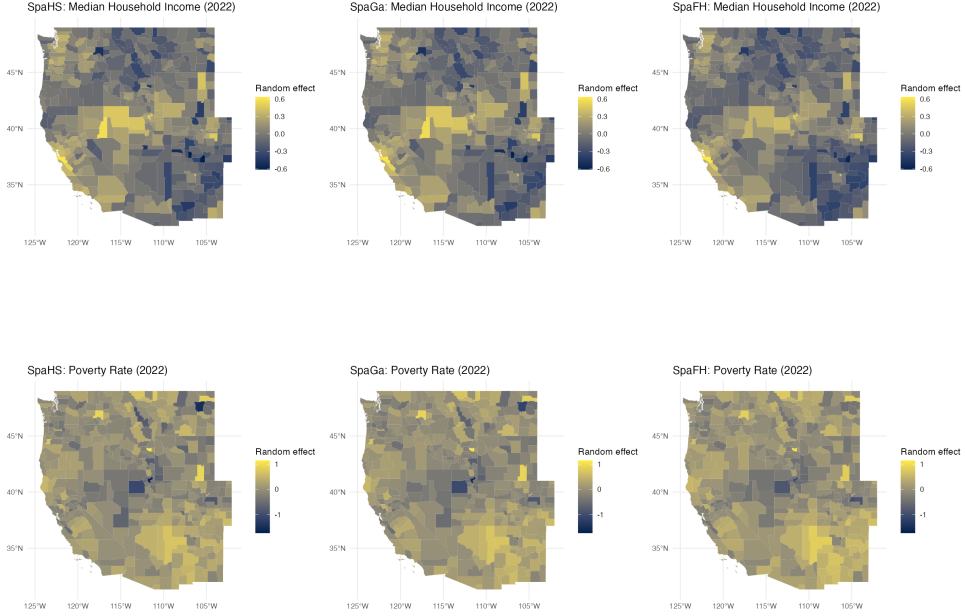


Figure 7: Spatial random effects on the log-scale of median household income and poverty rate for 413 counties in West Census Region, based on 5-year period estimates from the 2022 American Community Survey, including results from the SpaHS, SpaGa and SpaFH methods.

ber of posterior samples (10,000), on average, the MCMC sampling is considered efficient. Regarding computation time, the proposed methods are slower than the HS and FH approaches, mainly due to the increased number of latent variables. In SpaHS and SpaGa, the number of local parameters $\lambda_{i,j}$ is twice that of HS, and additional matrix operations required for modeling spatial dependence further increase computational cost. Several strategies could mitigate this computational burden, and these will be discussed in the Discussion section. However, addressing them in depth is beyond the scope of the present paper. All computations were performed on a laptop equipped with an Apple M1 Max processor and 32 GB of unified memory, running macOS 15.7.2 (build 24G325). Additional information on the real data analysis is provided in Appendix C.

6 Discussion

The proposed model becomes computationally challenging when applied to large-scale data. For instance, as the number of small areas grows, the size of the matrices to be inverted increases accordingly, leading to a higher computational burden. To address this issue, approximate infer-

Table 1: The Deviance Information Criterion (DIC) for various models, mean effective sample size (ESS) across components of small area mean θ and the CPU time, where the MCMC algorithm was run for 20,000 iterations, discarding the first 10,000 as burn-in.

Method	SpaHS	SpaGa	SpaFH	HS	FH
DIC	1625.31	1655.53	1684.29	1736.84	1649.78
ESS	8178.62	7685.26	9571.31	6972.30	9965.19
CPU time (min)	21.64	19.78	11.86	7.44	4.79

ence methods such as variational Bayes (Blei et al., 2017) or variational autoencoders (Kingma and Welling, 2013) could be considered as alternatives to MCMC. Indeed, such approaches have already been explored in the contexts of extreme value theory (Zhang et al., 2023) and small area estimation (Wang et al., 2025). Incorporating such approximate inference methods into the proposed framework remains an important direction for future research. The proposed prior can potentially be extended to spatially varying sparse coefficient models, where it may induce area-specific shrinkage of regression coefficients (Boehm Vock et al., 2015).

An interesting direction for future research would be to extend the current framework to allow for spatial correlation parameters that vary across regions, as proposed in the generalized multivariate CAR models by (Jin et al., 2005, 2007). Incorporating such flexibility could potentially capture local spatial heterogeneity more effectively. Extending the model to a spatio-temporal setting also presents another promising avenue, enabling the analysis of dynamic changes over both space and time. However, since computations based on MCMC are expected to be considerably demanding, some methodological or computational refinements will likely be required.

Acknowledgments

The authors' research was supported in part by JSPS KAKENHI Grant Numbers 25K07131 and 25K23108 from the Japan Society for the Promotion of Science. The authors also thank Dr. Xueying Tang of University of Arizona for sharing us R code of the paper Ghosh et al. (2022).

A Proof

Proof of Proposition 3.1. The joint posterior density is

$$\begin{aligned}\pi(\tilde{\mathbf{u}}, \boldsymbol{\beta}, \boldsymbol{\Sigma}, \boldsymbol{\Lambda}, \rho, \tau^2 \mid \mathbf{y}) &\propto \exp \left[-\frac{1}{2}(\mathbf{y} - \mathbf{X}\boldsymbol{\beta} - \boldsymbol{\Lambda}\tilde{\mathbf{u}})^\top \mathbf{V}^{-1}(\mathbf{y} - \mathbf{X}\boldsymbol{\beta} - \boldsymbol{\Lambda}\tilde{\mathbf{u}}) \right] \\ &\quad \times |\tau^2((\mathbf{D} - \rho\mathbf{W})^{-1} \otimes \boldsymbol{\Sigma})|^{-1/2} \exp \left[-\frac{1}{2}\tilde{\mathbf{u}}^\top \frac{1}{\tau^2}((\mathbf{D} - \rho\mathbf{W}) \otimes \boldsymbol{\Sigma}^{-1})\tilde{\mathbf{u}} \right] \\ &\quad \times \pi(\boldsymbol{\Sigma}) \left(\prod_{i=1}^m \prod_{j=1}^k \pi(\lambda_{i,j}) \right) \pi(\rho) \pi(\tau^2).\end{aligned}$$

Let $\mathbf{z} = \mathbf{y} - \boldsymbol{\Lambda}\tilde{\mathbf{u}}$. Then

$$\begin{aligned}(\mathbf{y} - \mathbf{X}\boldsymbol{\beta} - \boldsymbol{\Lambda}\tilde{\mathbf{u}})^\top \mathbf{V}^{-1}(\mathbf{y} - \mathbf{X}\boldsymbol{\beta} - \boldsymbol{\Lambda}\tilde{\mathbf{u}}) &= (\mathbf{z} - \mathbf{X}\boldsymbol{\beta})^\top \mathbf{V}^{-1}(\mathbf{z} - \mathbf{X}\boldsymbol{\beta}) \\ &= \mathbf{z}^\top \mathbf{V}^{-1/2}(\mathbf{I}_{mk} - \mathbf{P}_{\mathbf{X}})\mathbf{V}^{-1/2}\mathbf{z},\end{aligned}$$

where $\mathbf{P}_{\mathbf{X}} = \mathbf{X}(\mathbf{X}^\top \mathbf{V}^{-1} \mathbf{X})\mathbf{X}^\top$. Integrating $\pi(\tilde{\mathbf{u}}, \boldsymbol{\beta}, \boldsymbol{\Sigma}, \boldsymbol{\Lambda}, \rho, \tau^2 \mid \mathbf{y})$ with respect to $\boldsymbol{\beta}$, we have

$$\begin{aligned}\pi(\tilde{\mathbf{u}}, \boldsymbol{\Sigma}, \boldsymbol{\Lambda}, \rho, \tau^2 \mid \mathbf{y}) &= K \exp \left[-\frac{1}{2}(\mathbf{y} - \boldsymbol{\Lambda}\tilde{\mathbf{u}})^\top \mathbf{V}^{-1/2}(\mathbf{I}_{mk} - \mathbf{P}_{\mathbf{X}})\mathbf{V}^{-1/2}(\mathbf{y} - \boldsymbol{\Lambda}\tilde{\mathbf{u}}) \right] \\ &\quad \times |\tau^2((\mathbf{D} - \rho\mathbf{W})^{-1} \otimes \boldsymbol{\Sigma})|^{-1/2} \exp \left[-\frac{1}{2}\tilde{\mathbf{u}}^\top \frac{1}{\tau^2}((\mathbf{D} - \rho\mathbf{W}) \otimes \boldsymbol{\Sigma}^{-1})\tilde{\mathbf{u}} \right] \\ &\quad \times \pi(\boldsymbol{\Sigma}) \left(\prod_{i=1}^m \prod_{j=1}^k \pi(\lambda_{i,j}) \right) \pi(\rho) \pi(\tau^2) \\ &\leq K |\tau^2((\mathbf{D} - \rho\mathbf{W})^{-1} \otimes \boldsymbol{\Sigma})|^{-1/2} \exp \left[-\frac{1}{2}\tilde{\mathbf{u}}^\top \frac{1}{\tau^2}((\mathbf{D} - \rho\mathbf{W}) \otimes \boldsymbol{\Sigma}^{-1})\tilde{\mathbf{u}} \right] \\ &\quad \times \pi(\boldsymbol{\Sigma}) \left(\prod_{i=1}^m \prod_{j=1}^k \pi(\lambda_{i,j}) \right) \pi(\rho) \pi(\tau^2),\end{aligned}$$

where K is a positive constant. If the priors of $\boldsymbol{\Sigma}$, ρ , τ and λ_{ij} are proper, then the posterior density is proper.

□

B Additional information on posterior computation

We provide derivations of full conditional distributions, together with details of the sampling scheme for local parameters via the elliptical slice sampler.

B.1 Derivation of algorithm

- Sampling of regression coefficient vector β .

The full conditional density of β is given by

$$\begin{aligned}\pi(\beta \mid -) &\propto \exp \left[-\frac{1}{2}(\mathbf{y} - \mathbf{X}\beta - \Lambda \tilde{\mathbf{u}})^\top \mathbf{V}^{-1}(\mathbf{y} - \mathbf{X}\beta - \Lambda \tilde{\mathbf{u}}) \right] \\ &\propto \exp \left[-\frac{1}{2}(\mathbf{z} - \mathbf{X}\beta)^\top \mathbf{V}^{-1}(\mathbf{z} - \mathbf{X}\beta) \right] \quad (\mathbf{z} := \mathbf{y} - \Lambda \tilde{\mathbf{u}}), \\ &\propto \exp \left[-\frac{1}{2}(\beta - \mathbf{m})^\top (\mathbf{X}^\top \mathbf{V}^{-1} \mathbf{X})(\beta - \mathbf{m}) \right],\end{aligned}$$

where $\mathbf{y} \in \mathbb{R}^{mk}$, $\mathbf{X} \in \mathbb{R}^{mk \times s}$, $\beta \in \mathbb{R}^s$, $\tilde{\mathbf{u}}_i \in \mathbb{R}^{mk}$, $\Lambda = \text{blockdiag}(\Lambda_1, \dots, \Lambda_m) \in \mathbb{R}^{mk \times mk}$, $\mathbf{V} = \text{blockdiag}(\mathbf{V}_1, \dots, \mathbf{V}_m) \in \mathbb{R}^{mk \times mk}$ and

$$\mathbf{m} = (\mathbf{X}^\top \mathbf{V}^{-1} \mathbf{X})^{-1} \mathbf{X}^\top \mathbf{V}^{-1} \mathbf{z}, \quad \mathbf{z} := \mathbf{y} - \Lambda \tilde{\mathbf{u}}.$$

Hence, $\beta \mid - \sim \mathcal{N}_s(\mathbf{m}, (\mathbf{X}^\top \mathbf{V}^{-1} \mathbf{X})^{-1})$.

- Sampling of (transformed) random effect vector $\tilde{\mathbf{u}}$.

Using (3.5), the full conditional density of $\tilde{\mathbf{u}}$ is given by

$$\begin{aligned}\pi(\tilde{\mathbf{u}}_i \mid -) &\propto \exp \left[-\frac{1}{2}(\mathbf{y}_i - \mathbf{X}_i \beta - \Lambda_i \tilde{\mathbf{u}}_i)^\top \mathbf{V}_i^{-1}(\mathbf{y}_i - \mathbf{X}_i \beta - \Lambda_i \tilde{\mathbf{u}}_i) \right] \\ &\quad \times \exp \left(-\frac{1}{2}(\tilde{\mathbf{u}}_i - \boldsymbol{\mu}_{\text{CAR},i})^\top \boldsymbol{\Omega}_{\text{CAR},i}^{-1}(\tilde{\mathbf{u}}_i - \boldsymbol{\mu}_{\text{CAR},i}) \right) \\ &\propto \exp \left(-\frac{1}{2} \tilde{\mathbf{u}}_i^\top (\Lambda_i \mathbf{V}_i^{-1} \Lambda_i + \boldsymbol{\Omega}_{\text{CAR},i}^{-1}) \tilde{\mathbf{u}}_i + \tilde{\mathbf{u}}_i^\top (\Lambda_i \mathbf{V}_i^{-1} \boldsymbol{\xi}_i + \boldsymbol{\Omega}_{\text{CAR},i}^{-1} \boldsymbol{\mu}_{\text{CAR},i}) \right) \\ &\quad (\boldsymbol{\xi}_i := \mathbf{y}_i - \mathbf{X}_i \beta).\end{aligned}$$

where $\boldsymbol{\mu}_{\text{CAR},i} = \rho \sum_{j \sim i} \frac{1}{w_{i+}} \tilde{\mathbf{u}}_j$ and $\boldsymbol{\Omega}_{\text{CAR},i} = \frac{\tau^2}{w_{i+}} \boldsymbol{\Sigma}$. Hence, $\tilde{\mathbf{u}}_i \mid - \sim \mathcal{N}_k(\mathbf{A}^{-1} \mathbf{b}, \mathbf{A}^{-1})$,

where

$$\mathbf{A} = \boldsymbol{\Lambda}_i \mathbf{V}_i^{-1} \boldsymbol{\Lambda}_i + \boldsymbol{\Omega}_{\text{CAR},i}^{-1}, \quad \mathbf{b} = \boldsymbol{\Lambda}_i \mathbf{V}_i^{-1} \boldsymbol{\xi}_i + \boldsymbol{\Omega}_{\text{CAR},i}^{-1} \boldsymbol{\mu}_{\text{CAR},i}.$$

- Sampling of covariance matrix Σ .

Let $\tilde{\mathbf{U}} := (\mathbf{u}_1, \dots, \mathbf{u}_m) \in \mathbb{R}^{k \times m}$. We can also express as the matrix-normal distribution

$$\tilde{\mathbf{U}} \sim \mathcal{MN}_{k \times m}(\mathbf{O}, \boldsymbol{\Sigma}, \tau^2(\mathbf{D} - \rho \mathbf{W})^{-1})$$

whose density function is

$$\begin{aligned} f(\tilde{\mathbf{U}}) &= \frac{1}{(2\pi)^{km/2}} |\tau^2(\mathbf{D} - \rho \mathbf{W})^{-1}|^{-k/2} |\boldsymbol{\Sigma}|^{-m/2} \exp\left(-\frac{1}{2} \text{tr}\left[\frac{1}{\tau^2}(\mathbf{D} - \rho \mathbf{W}) \tilde{\mathbf{U}}^\top \boldsymbol{\Sigma}^{-1} \tilde{\mathbf{U}}\right]\right) \\ &\propto |\tau^2(\mathbf{D} - \rho \mathbf{W})^{-1}|^{-k/2} |\boldsymbol{\Sigma}|^{-m/2} \exp\left(-\frac{1}{2} \text{tr}\left[\frac{1}{\tau^2}(\mathbf{D} - \rho \mathbf{W}) \tilde{\mathbf{U}}^\top \boldsymbol{\Sigma}^{-1} \tilde{\mathbf{U}}\right]\right) \\ &\propto |\tau^2(\mathbf{D} - \rho \mathbf{W})^{-1}|^{-k/2} |\boldsymbol{\Sigma}|^{-m/2} \exp\left(-\frac{1}{2} \text{tr}\left[\tilde{\mathbf{U}} \frac{1}{\tau^2}(\mathbf{D} - \rho \mathbf{W}) \tilde{\mathbf{U}}^\top \boldsymbol{\Sigma}^{-1}\right]\right). \end{aligned} \tag{B.1}$$

Using (B.1), the full conditional density of $\boldsymbol{\Sigma}$ is given by

$$\begin{aligned} \pi(\boldsymbol{\Sigma} | \cdot) &\propto |\boldsymbol{\Sigma}|^{-m/2} \exp\left(-\frac{1}{2} \text{tr}\left[\tilde{\mathbf{U}}(\mathbf{D} - \rho \mathbf{W}) \tilde{\mathbf{U}}^\top \boldsymbol{\Sigma}^{-1}\right]\right) \\ &\quad \times |\boldsymbol{\Sigma}|^{-(\nu_0+k+1)/2} \exp\{-\text{tr}(\mathbf{B} \boldsymbol{\Sigma}^{-1})/2\} \\ &= |\boldsymbol{\Sigma}|^{-(m+\nu_0+k+1)/2} \exp\left[-\frac{1}{2} \text{tr}\left([\mathbf{B} + \tilde{\mathbf{U}} \frac{1}{\tau^2}(\mathbf{D} - \rho \mathbf{W}) \tilde{\mathbf{U}}^\top] \boldsymbol{\Sigma}^{-1}\right)\right]. \end{aligned}$$

Hence, $\boldsymbol{\Sigma} | \cdot \sim \text{IW}(m + \nu_0, \mathbf{B} + \tilde{\mathbf{U}} \frac{1}{\tau^2}(\mathbf{D} - \rho \mathbf{W}) \tilde{\mathbf{U}}^\top)$.

- Sampling of spatial correlation parameter ρ .

The full conditional density of ρ is given by

$$\pi(\rho | \cdot) \propto |\mathbf{D} - \rho \mathbf{W}|^{k/2} \times \exp\left[-\frac{1}{2} \tilde{\mathbf{u}}^\top \frac{1}{\tau^2}((\mathbf{D} - \rho \mathbf{W}) \otimes \boldsymbol{\Sigma}^{-1}) \tilde{\mathbf{u}}\right],$$

where we use the fact $|\tau^2((\mathbf{D} - \rho \mathbf{W})^{-1} \otimes \boldsymbol{\Sigma})| = (\tau^2)^{mk} |(\mathbf{D} - \rho \mathbf{W})^{-1}|^k |\boldsymbol{\Sigma}|^m$.

- Sampling of global/local parameters

- The full conditional distribution of Λ .

$$\begin{aligned}\pi(\boldsymbol{\lambda}_i \mid -) &\propto \exp \left[-\frac{1}{2} (\mathbf{y}_i - \mathbf{X}_i \boldsymbol{\beta} - \boldsymbol{\Lambda}_i \tilde{\mathbf{u}}_i)^\top \mathbf{V}_i^{-1} (\mathbf{y}_i - \mathbf{X}_i \boldsymbol{\beta} - \boldsymbol{\Lambda}_i \tilde{\mathbf{u}}_i) \right] \prod_{j=1}^k \pi(\lambda_{i,j}) \\ &= \exp \left[-\frac{1}{2} \left(\frac{\mathbf{y}_i - \mathbf{X}_i \boldsymbol{\beta}}{\tilde{\mathbf{u}}_i} - \boldsymbol{\lambda}_i \right)^\top \tilde{\mathbf{U}}_i \mathbf{V}_i^{-1} \tilde{\mathbf{U}}_i \left(\frac{\mathbf{y}_i - \mathbf{X}_i \boldsymbol{\beta}}{\tilde{\mathbf{u}}_i} - \boldsymbol{\lambda}_i \right) \right] \prod_{j=1}^k \pi(\lambda_{i,j}),\end{aligned}$$

where the fraction $\frac{\mathbf{y}_i - \mathbf{X}_i \boldsymbol{\beta}}{\tilde{\mathbf{u}}_i}$ is applied elementwise and $\tilde{\mathbf{U}}_i = \text{diag}(\tilde{v}_{i1}, \dots, \tilde{v}_{ik})$. Let

$$\boldsymbol{\mu}_{\boldsymbol{\lambda}_i} := \frac{\mathbf{y}_i - \mathbf{X}_i \boldsymbol{\beta}}{\tilde{\mathbf{u}}_i}, \quad \boldsymbol{\Omega}_{\boldsymbol{\lambda}_i} = (\tilde{\mathbf{U}}_i \mathbf{V}_i^{-1} \tilde{\mathbf{U}}_i)^{-1}.$$

- Sampling of τ^2 (horseshoe prior)

$$\pi(\tau^2 \mid -) \propto (\tau^2)^{-mk/2} \exp \left[-\frac{1}{2} \tilde{\mathbf{u}}^\top \frac{1}{\tau^2} ((\mathbf{D} - \rho \mathbf{W}) \otimes \boldsymbol{\Sigma}^{-1}) \tilde{\mathbf{u}} \right] \pi(\tau^2)$$

When $\tau \sim \text{C}_+(0, 1)$, using

$$\tau \sim \text{C}_+(0, 1) \iff \tau^2 \mid \psi \sim \text{IG}(1/2, 1/\psi), \quad \psi \sim \text{IG}(1/2, 1),$$

we have

$$\begin{aligned}\pi(\tau^2 \mid \psi, \text{others}) &\propto (\tau^2)^{-\frac{mk+1}{2}-1} \exp \left[-\frac{1}{\tau^2} \left(\frac{1}{2} \tilde{\mathbf{u}}^\top ((\mathbf{D} - \rho \mathbf{W}) \otimes \boldsymbol{\Sigma}^{-1}) \tilde{\mathbf{u}} + \frac{1}{\psi} \right) \right] \\ &\sim \text{IG} \left(\frac{mk+1}{2}, \frac{1}{2} \tilde{\mathbf{u}}^\top ((\mathbf{D} - \rho \mathbf{W}) \otimes \boldsymbol{\Sigma}^{-1}) \tilde{\mathbf{u}} + \frac{1}{\psi} \right), \\ \pi(\psi \mid \tau^2) &\propto \psi^{-1/2-1} \exp \left(-\frac{1}{\psi} \left(\frac{1}{\tau^2} + 1 \right) \right) \\ &\sim \text{IG} \left(\frac{1}{2}, \frac{1}{\tau^2} + 1 \right)\end{aligned}$$

- Sampling of a and b (normal-gamma prior)

Under the prior $a \sim U(0, 1)$ and $b \sim \text{Ga}(c, d)$, the full conditional densities for a and b are given by

$$\pi(b \mid -) \propto \left(\prod_{i=1}^m \prod_{j=1}^k b^a \exp(-b\lambda_{i,j}^2) \right) \times b^{c-1} \exp(-db)$$

$$\begin{aligned}
&= b^{(amk+c)-1} \exp \left(-b \left(\sum_{i=1}^m \sum_{j=1}^k \lambda_{i,j}^2 + d \right) \right) \\
&\sim \text{Ga} \left(amk + c, \sum_{i=1}^m \sum_{j=1}^k \lambda_{i,j}^2 + d \right), \\
\pi(a \mid -) &\propto \prod_{i=1}^m \prod_{j=1}^k \frac{b^a}{\Gamma(a)} \lambda_{i,j}^{2a-1} = \left(\frac{b^a}{\Gamma(a)} \right)^{mk} \left(\prod_{i=1}^m \prod_{j=1}^k \lambda_{i,j} \right)^{2a-1}.
\end{aligned}$$

B.2 Sampling of local parameter

We provide an overview of the elliptical slice sampler used for sampling $\lambda_1, \dots, \lambda_m$. For further details, the reader is referred to Murray et al. (2010) and Hahn et al. (2019). We define

$$\pi^*(\lambda_i) = \prod_{j=1}^k \left\{ \pi(\lambda_{ij}) \frac{1}{1 + \exp(-\eta \lambda_{ij})} \right\},$$

where η is a large constant (e.g., $\eta = 100$). For $i = 1, \dots, m$, let $\Delta_i = \lambda_i - \mu_{\lambda_i}$. Sampling is performed as follows.

1. Draw $\zeta_i \sim \mathcal{N}_k(\mathbf{0}, \Omega_{\lambda_i})$

Set $\zeta_{0i} = \Delta_i \sin \theta + \zeta_i \cos \theta$

Set $\mathbf{u}_{1i} = \Delta_i \cos \theta - \zeta_i \sin \theta$.

2. Draw ℓ from $\mathcal{U}(0, \pi^*(\mu_{\lambda_i} + \zeta_{0i} \sin \theta + \zeta_{1i} \cos \theta))$.

Initialize $a = 0$ and $b = 2\pi$.

2.1 Sample θ' from $\mathcal{U}(a, b)$.

2.2 If $\pi^*(\mu_{\lambda_i} + \zeta_{0i} \sin \theta' + \zeta_{1i} \cos \theta') > \ell$

Then: Set $\theta \leftarrow \theta'$. Go to step 3.

Else: If $\theta' < \theta$, set $a \leftarrow \theta'$, else set $b \leftarrow \theta'$. Go to step 2.1.

3. Return $\Delta_i = \zeta_{0i} \sin \theta + \zeta_{1i} \cos \theta$ and $\lambda_i = \mu_{\lambda_i} + \Delta_i$.

If we assume the horseshoe prior, we set $\pi(\lambda_{i,j}) = (2/\pi)(1 + \lambda_{i,j}^2)^{-1}$. When we use the normal-gamma type prior $\lambda_{i,j}^2 \sim \text{Ga}(a, b)$, we set $\pi(\lambda_{i,j}) = \frac{2b^a}{\Gamma(a)} \lambda_{i,j}^{2a-1} \exp(-b\lambda_{i,j}^2)$.

C Additional information on real data analysis

We present additional results from the data analysis described in Section 5.

We conduct an exploratory investigation of the shrinkage behavior of random effects under different models. As a benchmark, we first consider the Fay–Herriot (FH) model, which is the most basic among the competing methods. Let $e = \mathbf{y} - \mathbf{X}\hat{\beta}$ denote the marginal residuals under the FH model, where $\hat{\beta}$ is the posterior mean of β . The FH model is used as the baseline for no reason other than the fact that it is the most basic and widely used model in small area estimation. In the data analysis, the estimated regression coefficients were found to be almost identical across all the considered methods, and thus no noticeable differences were observed among the methods in terms of regression coefficient estimation. Note that e is not the usual regression residual; rather, it is obtained after marginalizing out the random effects. Thus, the analysis should be regarded as exploratory. From this perspective, e can be regarded as pseudo-data, and estimating random effects under sparse models may be interpreted as applying shrinkage to this pseudo-data. To examine the degree and structure of shrinkage, we analyze the sparsity patterns in e and their relationship with the estimated random effects.

Figure 8 presents a scatter plot of the two-dimensional residual vectors e . The color of each point represents a similarity measure between the two components of $e_i = (e_{i1}, e_{i2})$ (after normalization in each dimension). Specifically, we adopt a Bray–Curtis type similarity (Bray and Curtis, 1957) defined by

$$\delta_i = \frac{||e_{i1}| - |e_{i2}||}{|e_{i1}| + |e_{i2}|}, \quad \text{Similarity}_i = 1 - \delta_i$$

for $i = 1, \dots, m$. This measure takes values close to 1 when the absolute values of the two components are similar, and values close to 0 when they differ substantially. Points lying near the coordinate axes correspond to cases where one component is close to zero while the other is not, resulting in low similarity (blue). In contrast, points along the diagonal lines exhibit high similarity (red), indicating that the magnitudes of the two components are comparable. Based on this similarity measure, we divide the observations into groups with low similarity (one component sparse) and high similarity (both components sparse or both large), and investigate

how different methods shrink the random effects in each case.

We first consider the case where the similarity measure is at most 0.25, corresponding to observations whose components differ substantially. This setting represents situations in which sparsity is uneven across dimensions. Figure 9 displays scatter plots of e against the point estimates of the random effects obtained by SpaHS, SpaFH, and HS, shown separately for each dimension. The color indicates the value of the second component of e_i (poverty rate), which is shared across the panels. For observations colored in blue, where the second component is small, the first component (median household income) is close to zero. In this case, all methods shrink the estimated random effects toward zero in the first dimension. However, for the second dimension, both SpaFH and HS also shrink the estimates toward zero, even when the residual signal is present. This suggests that, since these methods perform shrinkage jointly across dimensions, a near-zero random effect in median household income leads to excessive shrinkage in poverty rate as well. In contrast, SpaHS mitigates this effect, exhibiting weaker shrinkage in the second dimension. A similar phenomenon is observed for the orange-colored points, where the poverty rate component is close to zero. Although all methods appropriately shrink the poverty rate effects, HS and SpaFH also excessively shrink the median household income effects, whereas SpaHS better preserves the nonzero signal.

Next, we examine the case where the similarity is at least 0.75, corresponding to observations whose components have similar magnitudes. The results are shown in Figure 10. These observations represent cases in which both components are either sparse or large. In this setting, HS and SpaHS yield similar shrinkage behavior, as both dimensions are shrunk or retained simultaneously. In particular, when the residuals are close to zero, the estimates are shrunk toward zero. For moderate residual values, the estimated random effects exhibit asymmetric shrinkage: for negative residuals, the estimates lie above the line $y = x$, while for positive residuals they lie below it. SpaFH, on the other hand, exhibits a noticeably different pattern from HS and SpaHS in this regime.

Although this analysis is exploratory in nature, the results consistently indicate that the proposed SpaHS method is capable of performing component-specific shrinkage of random effects. Through the real data analysis, we observe that SpaHS can adaptively shrink each component of the random-effect vector, thereby alleviating the over-shrinkage problem inherent

in models that impose common shrinkage across dimensions.

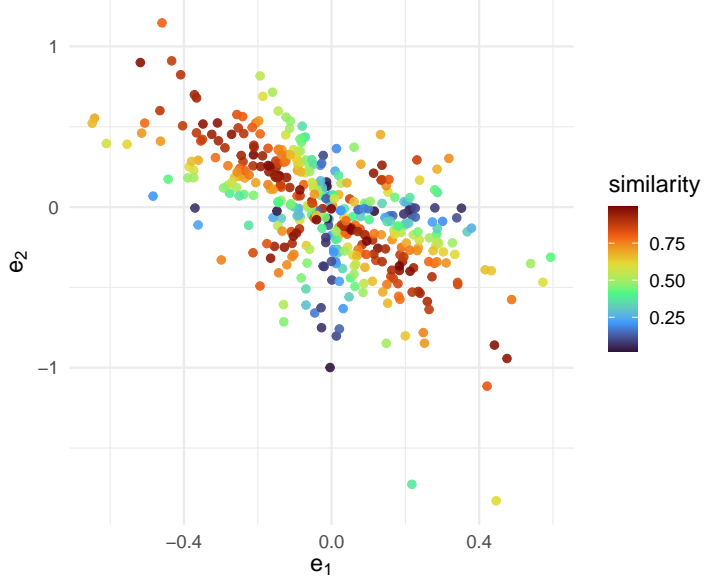


Figure 8: Scatter plot of the two-dimensional marginal residual $e_i = (e_{i1}, e_{i2})$ obtained under the Fay–Herriot (FH) model. Each point corresponds to a small area. The color indicates the similarity between the absolute values of the two components, defined by a Bray–Curtis type similarity $1 - \delta_i$, where $\delta_i = ||e_{i1}| - |e_{i2}|| / (|e_{i1}| + |e_{i2}|)$.

References

- Battese, G. E., R. M. Harter, and W. A. Fuller (1988). An error-components model for prediction of county crop areas using survey and satellite data. *Journal of the American Statistical Association* 83(401), 28–36.
- Benavent, R. and D. Morales (2016). Multivariate fay–herriot models for small area estimation. *Computational Statistics & Data Analysis* 94, 372–390.
- Bhattacharya, A., D. Pati, N. S. Pillai, and D. B. Dunson (2015). Dirichlet–laplace priors for optimal shrinkage. *Journal of the American Statistical Association* 110(512), 1479–1490.
- Blei, D. M., A. Kucukelbir, and J. D. McAuliffe (2017). Variational inference: A review for statisticians. *Journal of the American statistical Association* 112(518), 859–877.
- Boehm Vock, L. F., B. J. Reich, M. Fuentes, and F. Dominici (2015). Spatial variable selection

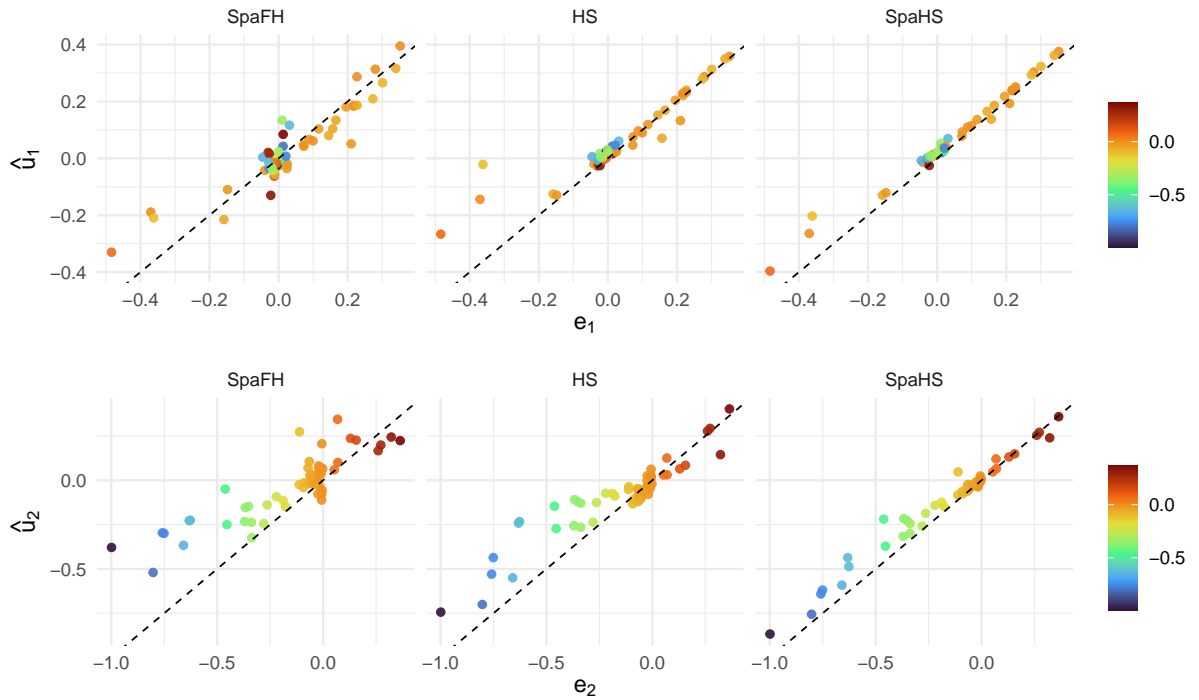


Figure 9: Scatter plots of the FH marginal residual $e_i = (e_{i1}, e_{i2})$ versus the estimated random effects under SpaHS, SpaFH, and HS, for areas with low similarity ($1 - \delta_i \leq 0.25$). These observations correspond to situations where sparsity is uneven across dimensions, that is, one component is close to zero while the other is nonzero. The upper and lower panels display the results for the first component (median household income) and the second component (poverty rate), respectively. Points are colored according to the value of the second residual component e_{i2} , with blue indicating values close to zero and orange indicating larger magnitudes.

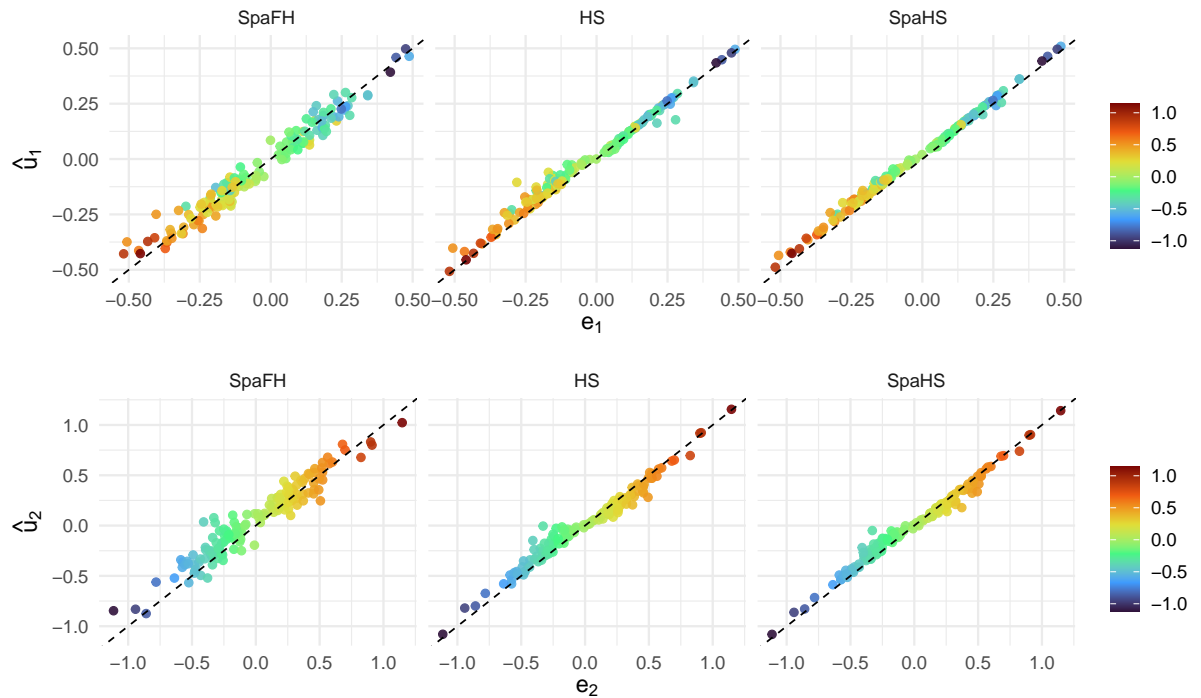


Figure 10: Scatter plots of the FH marginal residual $e_i = (e_{i1}, e_{i2})$ versus the estimated random effects under SpaHS, SpaFH, and HS, for areas with high similarity ($1 - \delta_i \geq 0.75$). These observations correspond to cases where both components of e_i are either small or large, indicating similar sparsity patterns across dimensions. As in Figure 9, the upper and lower panels show the first and second components, respectively, and points are colored according to the value of e_{i2} .

- methods for investigating acute health effects of fine particulate matter components. *Biometrics* 71(1), 167–177.
- Bray, J. R. and J. T. Curtis (1957). An ordination of the upland forest communities of southern Wisconsin. *Ecological Monographs* 27, 325–349.
- Carlin, B. P. and S. Banerjee (2003). Hierarchical multivariate car models for spatio-temporally correlated survival data. In *Bayesian Statistics 7: Proceedings of the Seventh Valencia International Meeting*. Oxford University Press.
- Carvalho, C. M., N. G. Polson, and J. G. Scott (2010). The horseshoe estimator for sparse signals. *Biometrika*, 465–480.
- Chakraborty, A., G. S. Datta, and A. Mandal (2016). A two-component normal mixture alternative to the fay-herriot model. *Statistics in Transition New Series* 17(1), 67–90.
- Chung, H. C. and G. S. Datta (2022). Bayesian spatial models for estimating means of sampled and non-sampled small areas. *Survey Methodology* 48(2), 463–489.
- Datta, G. S., B. Day, and T. Maiti (1998). Multivariate bayesian small area estimation: an application to survey and satellite data. *Sankhyā: The Indian Journal of Statistics, Series A*, 344–362.
- Datta, G. S., P. Hall, and A. Mandal (2011). Model selection by testing for the presence of small-area effects, and application to area-level data. *Journal of the American Statistical Association* 106(493), 362–374.
- Datta, G. S., P. Lahiri, T. Maiti, and K. L. Lu (1999). Hierarchical bayes estimation of unemployment rates for the states of the us. *Journal of the American Statistical Association* 94(448), 1074–1082.
- Datta, G. S. and A. Mandal (2015). Small area estimation with uncertain random effects. *Journal of the American Statistical Association* 110(512), 1735–1744.
- Datta, G. S., J. Rao, and D. D. Smith (2005). On measuring the variability of small area estimators under a basic area level model. *Biometrika* 92(1), 183–196.

- Fay, R. E. (1987). Application of multivariate regression to small domain estimation. *Small area statistics*, 91–102.
- Fay, R. E. and R. A. Herriot (1979). Estimates of income for small places: an application of james-stein procedures to census data. *Journal of the American Statistical Association* 74(366a), 269–277.
- Gelfand, A. E. and P. Vounatsou (2003). Proper multivariate conditional autoregressive models for spatial data analysis. *Biostatistics* 4(1), 11–15.
- Ghosh, T., M. Ghosh, J. J. Maples, and X. Tang (2022). Multivariate global-local priors for small area estimation. *Stats* 5(3), 673–688.
- Griffin, J. E. and P. J. Brown (2010). Inference with normal-gamma prior distributions in regression problems. *Bayesian Analysis* 5(1), 171–188.
- Hahn, P. R., J. He, and H. F. Lopes (2019). Efficient sampling for gaussian linear regression with arbitrary priors. *Journal of Computational and Graphical Statistics* 28(1), 142–154.
- Hamura, Y., K. Irie, and S. Sugasawa (2025). Outlier-robust bayesian multivariate analysis with correlation-intact sandwich mixture. *arXiv preprint arXiv:2508.18004*.
- Ito, T. and T. Kubokawa (2020). Robust estimation of mean squared error matrix of small area estimators in a multivariate fay–herriot model. *Japanese Journal of Statistics and Data Science* 3(1), 39–61.
- Ito, T. and T. Kubokawa (2021). Corrected empirical bayes confidence region in a multivariate fay–herriot model. *Journal of Statistical Planning and Inference* 211, 12–32.
- Jin, X., S. Banerjee, and B. P. Carlin (2007). Order-free co-regionalized areal data models with application to multiple-disease mapping. *Journal of the Royal Statistical Society Series B: Statistical Methodology* 69(5), 817–838.
- Jin, X., B. P. Carlin, and S. Banerjee (2005). Generalized hierarchical multivariate car models for areal data. *Biometrics* 61(4), 950–961.

Kingma, D. P. and M. Welling (2013). Auto-encoding variational bayes. *arXiv preprint arXiv:1312.6114*.

MacNab, Y. C. (2022). Bayesian disease mapping: Past, present, and future. *Spatial Statistics* 50, 100593.

Mardia, K. (1988). Multi-dimensional multivariate gaussian markov random fields with application to image processing. *Journal of Multivariate Analysis* 24(2), 265–284.

Murray, I., R. Adams, and D. MacKay (2010). Elliptical slice sampling. In *Proceedings of the Thirteenth International Conference on Artificial Intelligence and Statistics*, pp. 541–548. JMLR Workshop and Conference Proceedings.

Onizuka, T., F. Iwashige, and S. Hashimoto (2024). Bayesian boundary trend filtering. *Computational Statistics & Data Analysis* 191, 107889.

Park, T. and G. Casella (2008). The bayesian lasso. *Journal of the American Statistical Association* 103(482), 681–686.

Polson, N. G., J. G. Scott, and J. Windle (2013). Bayesian inference for logistic models using pólya–gamma latent variables. *Journal of the American statistical Association* 108(504), 1339–1349.

Porter, A. T., S. H. Holan, C. K. Wikle, and N. Cressie (2014). Spatial fay–herriot models for small area estimation with functional covariates. *Spatial Statistics* 10, 27–42.

Porter, A. T., C. K. Wikle, and S. H. Holan (2015). Small area estimation via multivariate fay–herriot models with latent spatial dependence. *Australian & New Zealand Journal of Statistics* 57(1), 15–29.

Rao, J. N. and I. Molina (2015). *Small area estimation*. John Wiley & Sons.

Ray, P., D. Pati, and A. Bhattacharya (2020). Efficient bayesian shape-restricted function estimation with constrained gaussian process priors. *Statistics and Computing* 30(4), 839–853.

- Spiegelhalter, D. J., N. G. Best, B. P. Carlin, and A. Van Der Linde (2002). Bayesian measures of model complexity and fit. *Journal of the Royal Statistical Society: Series B (Statistical Methodology)* 64(4), 583–639.
- Sugasawa, S. and T. Kubokawa (2020). Small area estimation with mixed models: a review. *Japanese Journal of Statistics and Data Science* 3(2), 693–720.
- Tang, X. and M. Ghosh (2023). Global-local priors for spatial small area estimation. *Calcutta Statistical Association Bulletin* 75(2), 141–154.
- Tang, X., M. Ghosh, N. S. Ha, and J. Sedransk (2018). Modeling random effects using global-local shrinkage priors in small area estimation. *Journal of the American Statistical Association* 113(524), 1476–1489.
- Tang, X. and L. Zhang (2024). A hierarchical gamma prior for modeling random effects in small area estimation. *Survey Methodology* 50(2), 287–301.
- Wang, Z., P. A. Parker, and S. H. Holan (2025). Variational autoencoded multivariate spatial fay-herriot models. *arXiv preprint arXiv:2503.14710*.
- Zhang, L., X. Ma, C. K. Wikle, and R. Huser (2023). Flexible and efficient spatial extremes emulation via variational autoencoders. *arXiv preprint arXiv:2307.08079*.